JOURNAL OF PETROLOGY

Journal of Petrology, 2016, Vol. 57, No. 11&12, 2163–2194
doi: 10.1093/petrology/egx001
Original Article

OXFORD

Causes of the Compositional Variability among Ocean Floor Basalts

Hugh St C. O'Neill[1] and Frances E. Jenner[2]*

[1]Research School of Earth Sciences, The Australian National University, Canberra, ACT 0200, Australia; [2]Department of Environment, Earth and Ecosystems, The Open University, Walton Hall, Milton Keynes MK7 6AA, UK

*Corresponding author. E-mail: frances.jenner@open.ac.uk

Received June 19, 2016; Accepted January 4, 2017

ABSTRACT

The chemistry of ocean floor basalts (OFB) has been much studied for the insights that the compositions of their parental magmas may give into the thermal structure of the mantle, and its compositional heterogeneity. But as Mike O'Hara pointed out, OFBs are not primary magmas, and their extensive low-pressure differentiation 'must be quantified before chemical features of lavas are ascribed to the nature of the underlying upper mantle'. O'Hara also emphasized that individual magmatic eruptions are products of complex magmatic systems. Volcanoes are not formed by isolated events, but are sites of long-term activity at which eruptions are caused by the arrival of replenishing magma that mixes with earlier magma through repeated cycles. In the intervals between replenishment events, part of the magma crystallizes, concentrating incompatible elements in the remaining magma. If the compositions of OFB are to be used to infer differences in the conditions of melting owing to mantle thermal structure, first it is necessary to disentangle the effects of this low-pressure evolution. It is a remarkable feature of OFB magmatism that these potentially complex replenish–mix–tap–crystallize (RMTX) cycles give rise to a simple pattern of chemical evolution when averaged at the global scale. Here we look at the deviations of 45 minor and trace element concentrations from these global average trends. The global trends are taken as the logarithms of the concentrations of the elements as a function of MgO concentration (log [M] vs [MgO]), and the deviations from these trends are defined as 'variabilities'. An element's variability is expected to result from a combination of source heterogeneity, partial melting in the mantle and melt extraction, and from the local variations in the RMTX process during crustal evolution. There is a strong correlation of an element's variability with its slope in the global average trend, where the slope is a proxy for the element's incompatibility (bulk partitioning) during global average RMTX. This correlation implies that the chemical controls on source heterogeneity and partial melting and melt extraction are similar to those during RMTX. Striking exceptions are the variabilities in plagioclase-hosted Na and Sr, indicating that a substantial part of the variability of Na in OFBs is due to variations in RMTX, rather than reflecting differences in extent of partial melting. If Iceland is excluded, there is no evidence from OFB chemistry to suppose that the distribution of potential temperatures in the sub-ridge mantle has a standard deviation, $\sigma(T_p)$, larger than about 10°C, and if variability of the mantle source composition is allowed for, $\sigma(T_p)$ could be even less. A principal component analysis of the variabilities reveals two more-or-less equally important principal components, suggesting that two distinct factors have affected incompatible trace element concentrations in global OFB. We suggest that these two factors are source heterogeneity and the RMTX process rather than the extent of partial melting or shape of the melting regime. An unexpected finding is the decoupling of the variabilities of very incompatible elements (VICE) such as Ba, Th and Nb, from those of the highly incompatible elements (HICE), such as La and the other light rare earth elements, Zr, P and Be.

Key words: ocean floor basalts; MORB; trace elements; major elements; mantle; magma mixing

INTRODUCTION

Over 50 years ago Mike O'Hara (O'Hara, 1965) showed that common tholeiitic basalts had compositions close to the low-pressure cotectic in the system SiO_2–$CaAl_2SiO_6$–Mg_2SiO_4–$CaMgSi_2O_6$, where the melt is multiply saturated with olivine, plagioclase, and clinopyroxene (ol + plag + cpx). Melting of the mantle would produce instead liquids with compositions at a higher pressure cotectic, where the equilibrium crystal phases would include orthopyroxene (i.e. ol + opx ± cpx). This observation precluded the hypothesis that tholeiites, despite their common occurrence in different tectonic settings, were 'the primary magma' or even 'a primary magma', as conceived by the geological theoreticians of previous generations.

At about the same time, it became apparent that the basalts of the oceanic crust were tholeiites too (Engel *et al.*, 1965). Originally these were called 'low-potassium tholeiites' to distinguish them from many of the already known tholeiites (like those from Hawaii), but with greater sampling it became apparent that their contents of incompatible trace elements such as K were quite variable, falling on a continuum from depleted to enriched. The continuum in the depletion–enrichment of the incompatible trace elements is well illustrated by the slopes of chondrite-normalized rare earth element (REE) patterns (O'Neill, 2016). These basalts have become known as 'mid-ocean ridge basalts' or MORB, but as similar basalts contributing to the oceanic crust are also produced elsewhere than at the mid-ocean constructive plate margins (e.g. by sea-floor spreading in marginal basins such as back-arc basins, along leaky transform faults, or the off-axis magmatism associated with some seamounts) the less specific name of 'ocean floor basalts' or OFB seems preferable (e.g. Cann, 1971). If, following O'Hara (1965, 1968), OFB are not primary melts, what has happened to them during their evolution from the melts extracted from the mantle, which might be called 'primary'? Here, Mike O'Hara's work has again had a profound influence. In a landmark paper (O'Hara, 1977), he pointed out that: 'A realistic model of volcanic plumbing predicts that most of the established major, trace and isotopic chemical features of the common basalts could have been imposed during magma evolution in high-level magma chambers, for which process there is extensive independent field and phase equilibria evidence'. He then added: 'These effects must be quantified before chemical features of lavas are ascribed to the nature of the underlying upper mantle.'

Although the field evidence for the evolution of OFB may have been sparse in the 1970s, there emerged at about this time ample other evidence that significant aspects of the geochemistry of OFB are the result of complex processes in their volcanic plumbing systems as envisaged by O'Hara (see also O'Hara & Mathews, 1981). A key part of this evidence was the over-enrichment of incompatible trace elements in suites of OFB samples (Bryan *et al.*, 1976; White & Bryan, 1977; Dungan & Rhodes, 1978; Rhodes *et al.*, 1979; Perfit *et al.*, 1983; Hekinian & Walker, 1987). This 'over-enrichment' refers to the observed increase in the concentrations of incompatible trace elements in a suite of samples compared with the increase that would be expected if the samples were related by partial crystallization, with the extent of the partial crystallization calculated from major element trends. The implication is that the calculation of the extent of crystallization must be based on erroneous assumptions. One potential point of confusion is that the term 'enriched' is widely used in another context in basalt geochemistry, which is to refer to the overall pattern of the incompatible trace elements, as seen when normalized to some standard such as the Bulk Silicate Earth composition. Thus an OFB might, for example, be characterized as 'incompatible element enriched' or 'light rare earth element enriched' to distinguish it from the more usual OFB, which are 'depleted' or 'light rare earth element depleted'. This 'enriched/depleted' designation may be applied to a single sample; 'over-enrichment' is a phenomenon observable only in a suite of samples, with reference to some parental composition that may itself be 'enriched' or 'depleted'.

O'Neill & Jenner (2012) showed that the over-enrichment phenomenon is not confined to individual suites, but characterizes the average behaviour of OFB at the global scale. They proposed that its explanation lies in the effects of the volcanic plumbing systems, as predicted by O'Hara (1977), operating as an integral part of the magmatism that forms the oceanic crust. The essential features of the process may be thought of as occurring over cycles composed of the following steps (O'Neill & Jenner, 2012; Coogan & O'Hara, 2015).

1. Magma separates from its upwelling mantle source and moves upwards into the crust (two-phase flow; see, e.g. McKenzie, 1984).
2. In the crust, this 'parental' magma mixes with magma from previous cycles; the latter is multiply saturated with phases on the tholeiitic low-pressure cotectic (ol + plag + cpx). Mixing of the parental and evolved melt pushes the liquid away from the ol + plag + cpx cotectic into the ol primary phase volume.
3. A portion of the mixed magma erupts, which is the basaltic material sampled from the sea floor during dredging. The fraction of the magma chamber tapped in each cycle is denoted ϕ_T.
4. The untapped portion of the magma undergoes crystallization, returning the liquid composition to the low-pressure cotectic. The crystallized material forms the gabbroic lower part of the oceanic crust, which is sampled during drilling of the sea floor. The fraction of the magma chamber crystallized in each cycle is denoted ϕ_X.

In summary, the magma in the volcanic plumbing system at mid-ocean ridges is replenished, mixed, then

tapped, after which it partially crystallizes (X); hence, the process is referred to as RMTX (or RTX if mixing is taken for granted). The part of the volcanic plumbing system where the mixing and crystallization takes place has commonly been referred to as the 'magma chamber', but this term should be understood in this context as having no implications for size or shape. On the basis of seismic constraints (or lack thereof) the magma at oceanic spreading centres occurs in thin sills that are <1–2 km wide and only a few tens to a few hundreds of meters thick (Sinton & Detrick, 1992; Marsh, 2007). The presumed architecture of the oceanic crust implies that it is built up by crystallization from a trans-crustal series of such bodies, with residual liquid expressed at the surface to form the OFB that make up the top of the magmatic crust. The complexity implied for the evolution of the magma within such a crustal system is great, but we propose that many of the essential features of this evolution may be usefully understood by conceptually simplifying the process to one occurring within one volume, called the 'magma chamber', operating at some notional pressure that approximates the range of pressures over which the crustal evolution of the parental magma actually occurs (e.g. Rubin & Sinton, 2007).

O'Hara (1977) and O'Hara & Mathews (1981) showed that the chemical composition of the magmas emerging from this kind of idealized replenished magma chamber could be described by simple mass-balance equations if the magma chamber were to evolve to a steady state, which is an idealization on top of an idealization. Subsequently, Albarède (1985) pointed out that the equations at steady state differed considerably for compatible elements depending on whether mixing and tapping followed or preceded crystallization, and it was with the latter option (i.e. RMTX not RMXT) that O'Neill & Jenner (2012) were able to describe the average global differentiation trend of OFB.

O'Neill & Jenner (2012) took as their starting point the observation that the average trace element concentrations in the global array of OFB glasses followed the relationship

$$\log[\mathrm{M}] = \log[\mathrm{M}]_o + \text{slope}\ ([\mathrm{MgO}] - 10) \qquad (1)$$

where the square brackets denote concentration, $[M]_o$ is the concentration of a trace element in a parental magma, taken to be 10 wt% MgO, based on the approximate [MgO] of the bulk oceanic crust (White & Klein, 2014) and various other petrological and experimental considerations (see O'Neill & Jenner, 2012, and references therein). [MgO] monitors the extent of low-pressure evolution, as it is a good proxy for liquidus temperature in olivine-saturated, volatile-poor basalts (e.g. Putirka, 2008). Sometimes Mg# or its equivalents $MgO/Fe^{2+}O$ or MgO/FeO_t (where FeO_t is total Fe recalculated as $Fe^{2+}O$) is used instead for this purpose, but this usage convolutes three thermodynamic components (MgO, $Fe^{2+}O$ and $Fe^{3+}O_{1.5}$) and carries the danger of imposing preconceived notions that OFB evolve by partial crystallization without replenishment. There is also the practical problem that defining these variables requires taking some view on what to do about the two oxidation states of Fe.

O'Neill & Jenner (2012) then showed that the average behaviour of [M] as described by equation (1) could be explained by an idealized, average RMTX process. The idealized process starts from a single parental composition, and has the cycles of replenishment, tapping and fractionation occurring in a regular sequence, with the amount of replenishing magma the same in each cycle, as are the fractions of magma tapped and crystallized. Each magma chamber is assumed to have reached steady state.

The average behaviour of the global ensemble of idealized magma chambers is characterized by a specific relationship between the fraction tapped ($\overline{\phi_T}$) and fraction crystallized ($\overline{\phi_X}$), the play-off between the values of which determines the [MgO] of the tapped liquid. Here the bars above the symbols are used to denote global average values; individual magmatic plumbing systems may be expected to have fractions tapped (ϕ_T) and crystallized (ϕ_X) that vary about the global average. The tapped liquid has a major element composition that is a mix between the cotectic liquid of the magma chamber and the replenishing, parental liquid. Hence, whereas the major element composition of the crystallizing magma is buffered by the cotectic, the tapped magma is displaced from this cotectic according to the fraction of replenishing magma added in each cycle. From a geochemical point of view, the most important feature of the model is that the incompatible trace elements are buffered differently from the major elements, by the balance between ϕ_T and ϕ_X. In the case of a perfectly incompatible trace element (one with bulk crystal–melt partition coefficient of zero), it is easy to visualize that the balance is achieved when the amount of an element that is lost in the erupted magma equals the amount input by the replenishing magma. The number of cycles needed to reach steady state depends on ϕ_T and ϕ_X and the incompatibility of the element (Albarède, 1985), being largest for the perfectly incompatible trace elements.

Deviations from any aspect of this idealized behaviour cause variability about the average global trend. If the concentration of an element on the global trend at a specific [MgO] is $[M]_{calc}$, (given by $\log [M]_{calc} = \log[M]_o + \text{slope}\ ([MgO] - 10)$), then the variability of M is defined as

$$\sigma(\log[\mathrm{M}]) = \left(\frac{\Sigma(\log[\mathrm{M}] - \log[\mathrm{M}]_{calc})^2}{n}\right)^{1/2}. \qquad (2)$$

As may be seen from the foregoing discussion, this variability could be built up from many factors, which may be grouped for convenience into three categories, as follows.

1. Variability inherited from the variability of the parental magmas, arising from variable source compositions, or degree of partial melting.

2. Deviations from the idealized, steady-state, regular-cycle RMTX process.
3. Variations in the characteristics of the magma chambers making up the global ensemble, including deviations from the global relationship between $\overline{\phi_T}$ and $\overline{\phi_X}$, or the proportions of the cotectic phases (ol, plag, cpx) in the magma chamber. These latter vary with the pressure of the magma chamber (e.g. Presnall *et al.*, 1978).

Of these categories, much attention has focused on the variability in the parental magmas, because of the potential that the chemistry of these magmas may reflect the thermal structure of the mantle, through difference in the degree of partial melting (Klein & Langmuir, 1987, 1989; McKenzie & Bickle, 1988; Niu & Batiza, 1991; Langmuir *et al.*, 1992; Dalton *et al.*, 2014; Gale *et al.*, 2014). It is, however, widely recognized that mantle thermal structure alone cannot be the only cause of compositional variability in the parental magmas, with source composition playing a major role at least for the more incompatible trace elements. For example, the heterogeneity of isotopic compositions in the daughter elements of radiogenic isotope systems (i.e. Sr, Nd, Hf and Pb isotopes) must be inherited from compositional variability in the parent/daughter ratios of the relevant elements in the mantle sources of OFB (e.g. Hofmann, 2003; Stracke, 2012, and references therein). However, these radiogenic isotopic systems mostly involve incompatible trace elements, except for Re/Os, which are a pair of compatible elements whose behaviour is controlled by minor accessory phases (sulfide ± alloys). Hence, these systems do not directly address the question of major element variability in the source, an extreme case of which is lithological variability, such as mixtures of peridotite and pyroxenite, which have been proposed from time to time to explain various aspects of OFB chemistry (e.g. Salters & Hart, 1989; Hirschmann & Stolper, 1996; Sobolev *et al.*, 2007). Physical factors other than temperature, such as the rates of upwelling or sea-floor spreading, may also contribute to chemical variability (e.g. Rubin & Sinton, 2007). The question is then, what proportions of an element's variability in OFB are to be assigned to the different contributing factors? As any likely assignment must include source composition as an important contributing factor (from the evidence of the radiogenic isotope heterogeneity), this raises the further question of how the OFB source mantle acquired its variability. Although the radiogenic isotopes can help with this question by addressing the time dimension of the process (or processes), they provide only a partial perspective of how it happened, because of the aforementioned limitation that the parent–daughter pairs sample only a fairly restricted range of chemical properties compared with the full suite of major and trace elements.

A major problem is that the parental magmas are not directly observed, as O'Hara (1965, 1968) showed. Consequently, any attempt to use actual OFB compositions to place constraints on the thermal, mineralogical or chemical state of the source mantle needs to account for the variability introduced during their crustal evolution, controlled by the processes listed in categories (2) and (3) above. For incompatible trace elements, it has often been claimed that the crustal evolution of the magmas would have only a minor influence on incompatible element variability. The claim rests on deductive reasoning starting from the premise that this crustal evolution occurs by closed-system crystallization (fractional or equilibrium), which is not effective in fractionating incompatible element ratios (White & Schilling, 1978). Therefore, by this deductive reasoning, any observed variability of incompatible element ratios would have to be ascribed to the variability in the parental magmas (see also Hofmann, 2003, and references therein). This premise has achieved a status of such commonplace familiarity that it often escapes examination and, consequently, representative compositions for global OFB are directly used to place constraints on the composition and evolution of the OFB-source depleted mantle (Salters & Stracke, 2004; Arevalo & McDonough, 2010; Gale *et al.*, 2013). If, however, crustal evolution of OFB magmas occurs by the RMTX process rather than by closed-system simple fractional crystallization (SFX), this deductive reasoning is obviated, for RMTX is effective at fractionating all but the most incompatible of the incompatible trace elements (O'Neill & Jenner, 2012). One consequence of ignoring the possibility of RMTX is that attempts at mapping geochemical variability in global OFB onto differences in the degree of melting and hence mantle temperature variations will overestimate the latter.

Here we revisit the causes of compositional variability in ocean floor basalts. We show that there are systematics in the global variability of the incompatible trace elements that constrain the apportioning of this variability between source composition, melting processes (including mantle temperature variations) and low-pressure, crustal evolution, potentially revealing much about not only OFB petrogenesis but also the history of mantle.

THE PETROLOGICAL CONTEXT

In the following discussion, the term 'oceanic crust' will be used to refer to the magmatic part of the oceanic crust, ignoring the sedimentary veneer on top (layer 1) and the effects of syn- and post-igneous hydrothermal alteration and metamorphism (see, e.g. Plank, 2014; Staudigel, 2014; White & Klein, 2014). The melt forming the oceanic crust is produced beneath rifting margins by decompression melting as mantle upwells, which is itself caused in part by the viscous drag of the plates moving apart (e.g. McKenzie & Bickle, 1988). The thickness of normal crust away from anomalous regions (including fracture zones and areas with plume-related temperature anomalies) has been estimated as 7·1 ± 0·8 km (White *et al.*, 1992), later revised to 6·3 ± 0·9 km (White *et al.*,

1992; Bown & White, 1994). According to the parameterization by Langmuir *et al.* (1992) of mantle melting owing to passive adiabatic upwelling, this normal crustal thickness corresponds to an average degree of melting, $\overline{F}_{OFB}$, of 0·110 ± 0·007 (see fig. 5 of Langmuir *et al.*, 1992).

In typical oceanic crust, the top few hundred meters is made up of basaltic pillow lavas (ocean floor basalts or OFB), overlying 1–1·5 km of hypabyssal dolerite dikes and sheets, with the remainder being coarser grained mafic rock broadly described by the term 'gabbro' (White & Klein, 2014). Much of this 'gabbro' is of cumulate origin (Coogan, 2014), and is complementary to the basalt: crystallization of the parental liquids gives rise to residual liquids, the basalts and dolerites, and the crystallized solids, the 'gabbros'. The composition of a parental liquid is therefore potentially recoverable from a section through the crust by adding the basalts and their hypabyssal equivalents to the 'gabbros' according to their proportions in the crustal section (e.g. Pallister, 1984; Gillis *et al.*, 2014). The term 'gabbro' was used in quotation marks in the previous sentences for a good reason. Although these rocks are indeed often gabbros (usually olivine gabbros), the cumulates also include troctolites, and other rocks with variable proportions of olivine to plagioclase to clinopyroxene, sometimes even orthopyroxene (Gillis *et al.*, 2014), which precludes them from being called 'gabbro' *sensu stricto.* As the cumulates are layered, the scale of the layering raises difficulties of nomenclature because there is choice in what to take as a lithological unit.

Cumulate dunites are present in ophiolite sections from suprasubduction-zone settings (e.g. Pirard *et al.*, 2013), but how much cumulate dunite occurs in more typical lower oceanic crust is poorly known. This is an important question, because the amount of cumulate dunite corresponds to the extent of olivine-only crystallization from the mantle-derived magmas, which is a salient expression of the average depth of partial melting, but is also sensitive to H_2O contents. Just as 'gabbro' serves to denote the products of crystallization, 'basalt' can be taken to refer to the rocks formed from the residual liquids; that is, not only the erupted basalts but also their hyperbyssal equivalents, dolerite and any gabbro of non-cumulate origin that could also be called coarse-grained dolerite.

Very few ocean floor drilling projects have penetrated into the lower crust and none have recovered cores for the entire lower crustal section—a summary of the findings from various ocean floor drilling programmes has been given by Coogan (2014). Hence the evidence for our view of 'normal' ocean crust structure comes mainly from seismological studies, whose interpretation has been informed by examination of the ocean crust sections of ophiolites. However, seismology is more sensitive to such things as porosity and hydrothermal alteration than it is to lithology. Another problem is that ophiolites may not be typical of the oceanic crust. Ophiolites, perhaps with a few arguable exceptions, seem to have been generated at back-arc basin spreading centres and appear to have more hydrous and/or oxidized parental melt compositions compared with OFB parental magmas (e.g. Searle & Cox, 1999; Pirard *et al.*, 2013). Because there are major differences in the crystallization sequences of 'wet' versus 'dry' melts (e.g. Perfit *et al.*, 1980; Arculus, 2004), the cumulate portions of ophiolites are less than perfect analogues for the lower oceanic crust.

Seismology does not distinguish between gabbros of cumulate or residual origin, which are complementary to the basalts, dolerites and gabbros that are essentially coarse-grained dolerites, so that seismologically defined 'gabbros' do not correspond faithfully to the distinction between 'basalt' and residual 'gabbro' that one would like to define for petrogenetic purposes. The lithological structure of the lower crust appears to be extremely complex, and the gabbros of the lower crust may interleave with mantle peridotite (e.g. Cannat, 1996), refuting the possibility of an exact definition of crustal thickness. The problem becomes even more acute where thick dunite sections occur, like those described by Pirard *et al.* (2013). These factors prevent a precise evaluation of how much cumulate has been subtracted from the parental magmas to form the basalts and their hypabyssal equivalents, but at present it seems that the oceanic crust is typically about 25% basalt plus dolerite and 75% residual gabbro. Cumulate gabbros make up 66% of the Oman ophiolite according to Pallister (1984), although like most or possibly all ophiolite sections, this crust is from a suprasubduction environment (Searle & Cox, 1999). For oceanic crust that may be more representative of that produced at mid-ocean ridges, Gillis *et al.* (2014) suggested that the Hess Deep section includes 22·5 ± 4·5% of upper 'basaltic' crust.

Despite representing only a subordinate fraction of the mantle-derived parental melts, the erupted basalts provide most of the information about these melts, with much of this information coming from the glassy fragments of the rinds of lava pillows, which are produced by rapid quenching as the lava erupts into seawater. These glassy rinds have been much sampled by dredging, and are readily analysable (e.g. Melson *et al.*, 2002; Arevalo & McDonough, 2010; Jenner & O'Neill, 2012*a*). Glasses also have the advantage of being liquid compositions not affected by crystal accumulation, and on account of their rapid quenching they commonly retain their volatiles during eruption (e.g. Le Voyer *et al.*, 2015; Jenner & Arevalo, 2016, and references therein). The problem is then to relate these well-studied glass compositions (and, if needed, related whole-rock basalt compositions) to their parental magma compositions.

PARENTAL OFB MELT COMPOSITIONS

The average composition of the magmas parental to OFB has been postulated to have about 10·5 ± 0·5 wt % MgO (McKenzie & Bickle, 1988; Niu & Batiza, 1991; O'Neill & Jenner, 2012). Pallister (1984) estimated the

average composition of the Semail ophiolite to be slightly lower (9·2 wt %), with the cumulus gabbro section having 10·3 wt % MgO. From the available data Coogan (2014) reported the average and standard deviation for the lower crustal (non-basaltic) part of the oceanic crust as 9·4 ± 1·1 wt % MgO, but said: 'This should be considered a very approximate value (note the large standard deviations about the average) and is unlikely to be representative of the global average composition of the lower oceanic crust as its Mg# is too low.' Recently, Gillis *et al.* (2014) have integrated dredged basalt compositions with the deeper gabbroic crustal components sampled by drilling at the Hess Deep rift, to obtain 12·1 wt % MgO.

Some petrologists have argued that the parental magmas have higher [MgO], with ≥ 14 wt % suggested (Green *et al.*, 2001; Falloon *et al.*, 2007). The importance of this view is that it bears on the potential temperatures of the mantle: higher MgO basalts imply deeper melting, therefore higher potential temperature. Owing to the expansion of the primary phase volume of olivine with decreasing pressure in basalt phase diagrams, such higher pressure MgO-rich melts have only olivine (± minor Cr-spinel) on their liquidus at crustal pressures, and the crystallization interval before plagioclase joins olivine on the liquidus will increase monotonically with the average pressure of melting. The ratio of olivine to Cr-spinel on the olivine + Cr-spinel cotectic of tholeiites is about 100 according to Roeder *et al.* (2006), so the presence of the spinel may be ignored except for the element Cr. As pointed out above, the amount of cumulate dunite from olivine-only crystallization in normal oceanic crust is poorly known, so at present the extent of olivine-only crystallization cannot be constrained from field observations.

The proportion of cumulate gabbro in the 6·3 ± 0·9 km of typical oceanic crust must be a key item in understanding OFB petrogenesis. The average [MgO] of sampled OFB is estimated at about 7·6 wt % (Gale *et al.*, 2013) or 7·8 wt % (Arevalo & McDonough, 2010; Gale *et al.*, 2014), which requires less than 40% fractional crystallization from a likely parental magma with 10·5 wt % MgO (e.g. O'Neill & Jenner, 2012, fig. 1c). An extra few per cent olivine would be added to this if the parental magma had higher [MgO]. This amount of crystallization predicts an oceanic crust with 60% basalt plus hypabyssal equivalents and 40% cumulate gabbros, rather than the 25–75% inferred from seismology and ophiolite sections. A not unrelated issue is the scarcity of highly evolved compositions among the global database of OFB. Such compositions should be common for average extents of fractional crystallization of 75% or more of parental magma, but, of the 9050 OFB glasses in the Smithsonian Abyssal Volcanic Glass data file (Melson *et al.*, 2002), only 3·8% have less than 5·0 wt % MgO. Why does the average MORB have about 7·6 wt % MgO anyway? An early suggestion was that the preponderance of MORB in the range 7–8 wt % MgO (Fig. 1a) was because of density filtering, with this compositional range lying at a minimum in a plot of density

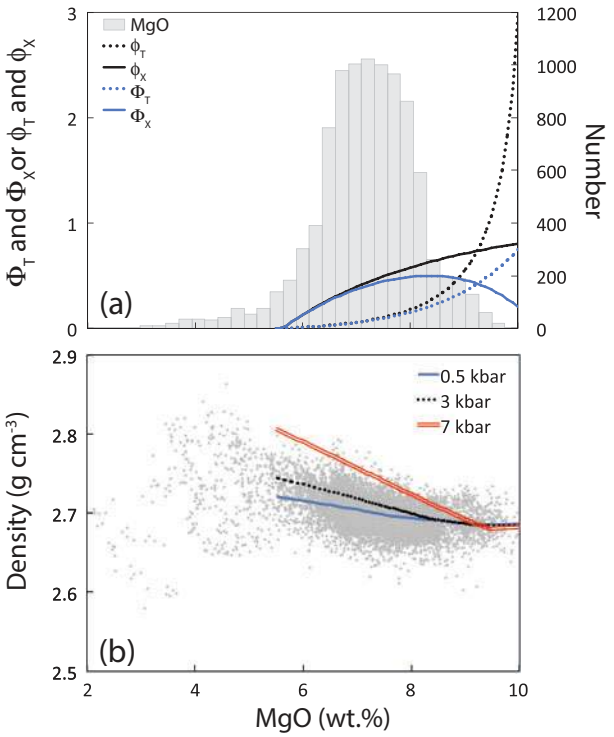

Fig. 1. (a) Histogram of MgO concentrations in the Smithsonian Abyssal Volcanic Glass Database (Melson *et al.*, 2002) compared with the solution of the steady-state magma chamber model of O'Neill & Jenner (2012) with fraction tapped (ϕ_T or Φ_T) or crystallized (ϕ_X or Φ_X) in each cycle. ϕ_T and ϕ_X are as defined by Albarède (1985) whereas Φ_T and Φ_X are as defined by O'Hara & Herzberg (2002) and used by Coogan & O'Hara (2015). (b) The densities of the Smithsonian Abyssal Volcanic Glass Database samples calculated using the model of Lange & Carmichael (1987) with temperatures calculated using equation (14) from Putirka (2008). Modelling curves were calculated using Petrolog (Danyushevsky & Plechov, 2011) from the starting compositions given by O'Neill & Jenner (2012) and calculated at 0·5, 3 and 7 kbar.

versus [MgO] (Sparks *et al.*, 1980; Stolper, 1980), but estimates of silicate melt densities (Lange & Carmichael, 1987) show that the density minimum in OFB occurs at substantially higher MgO, around 9–10 wt % (Fig. 1b).

Another problem occurs with interpreting the phenocryst assemblages in erupted OFB, which usually do not reflect cotectic proportions (Coogan, 2014). Clinopyroxene phenocrysts are egregiously rare in OFB, a phenomenon referred to as the 'clinopyroxene paradox' (Francis, 1986). Moreover, the olivine and plagioclase phenocrysts are often out of equilibrium with their host magma (Coogan, 2014, fig. 5). *Ad hoc* explanations might be found for these observations if they are taken one by one, but when considered together they point to the influence of the volcanic plumbing system in determining OFB compositions by the RMTX process or its variants.

REPLENISH–MIX–TAP–CRYSTALLIZE (RMTX)

O'Hara (1977) emphasized that eruptions of basalt are not isolated events, but occur as episodes within a

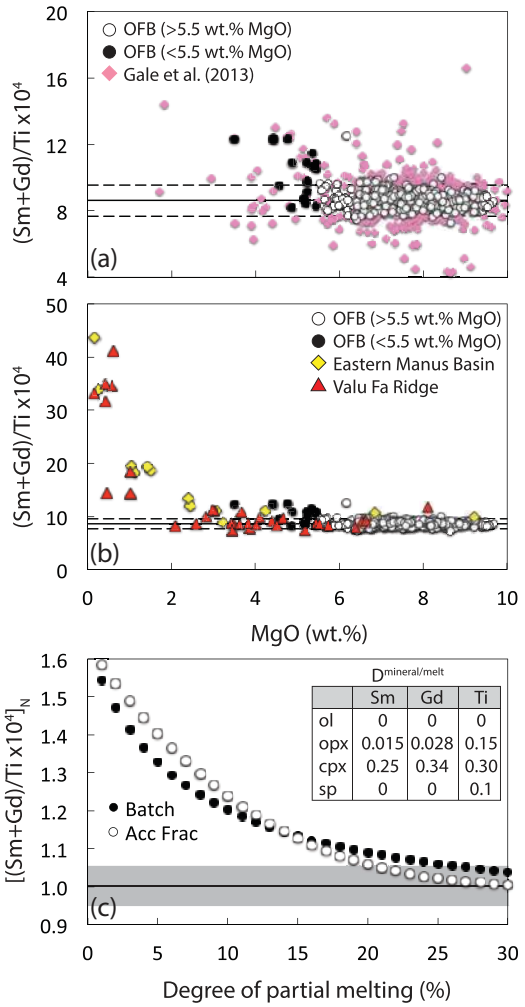

Fig. 2. (a, b) Variations in (Sm + Gd)/Ti vs MgO. (a) Global OFB datasets of Jenner & O'Neill (2012*a*) and Gale *et al.* (2013). The continuous line is the average for data from Jenner & O'Neill (2012*a*) with >5·5 wt % MgO and the dashed lines show ± 2σ about the average. (b) OFB datasets of Jenner & O'Neill (2012*a*) vs back-arc basin magmas from the SW Pacific (Jenner *et al.*, 2010, 2015). The large increase in (Sm + Gd)/Ti vs MgO at ~4 wt % MgO for back-arc basin magmas marks the onset of crystallization of Fe–Ti oxides. The almost constant (Sm + Gd)/Ti of OFB for samples with > 5·5 wt % MgO implies that mixing in of highly evolved melts (i.e. saturated in Fe–Ti oxides) in causing the over-enrichments in the incompatible elements of OFB is unlikely to be contributing to the average global OFB patterns. (c) Calculated (Sm + Gd)/Ti as a function of degree of partial melting (*F*), normalized (N) to the ratio in the source, assuming isobaric batch (Batch) or accumulated fractional (Acc Frac) melting of spinel lherzolite. The initial mode is from O'Neill (2016), and the melting reaction is from Niu (1997). Partition coefficients for olivine are from O'Neill & Jenner (2012), for clinopyroxene and orthopyroxene from Yao *et al.* (2012) for Sm and Gd, and from Mallmann & O'Neill (2009) for Ti. The decrease in (Sm + Gd)/Ti with *F* is due to the difference in the partitioning of Sm and Gd compared with Ti between clinopyroxene and orthopyroxene and the progressive melting out of clinopyroxene relative to orthopyroxene, and as such is not expected to be sensitive to the melting model. The small standard deviation of the ratio of (Sm + Gd)/Ti observed in OFB of 5·4%, shown by the grey band of ± 5·4% around the source ratio, implies a relatively high global average *F* and a small global σ(*F*) during partial melting. The ratio of (Sm + Gd)/Ti in parental melts is preserved during subsequent crustal evolution, whether by SFX or by RMTX, because the bulk partition behavior of both (Sm + Gd) and Ti are controlled only by clinopyroxene in the absence of a low-Ca pyroxene.

long-term process that builds structures like volcanoes. The oceanic crust, like any volcanic system, is built up through many eruptions, such that vertical sections through the uppermost crust are composed of flows spanning many thousands of years (e.g. Brandl *et al.*, 2016). A mid-ocean ridge is usually pictured as the place where magma is received in pulses from the decompression melting [called 'magmons' by Scott & Stevenson (1986)], to be distributed to form the crust on top of the diverging plates, with a fraction ϕ_T of basalt and dolerite, and ϕ_X of cumulate gabbros. Each magmon rises to a place where previous magmons, probably very many previous magmons, have been. There appears to be no theoretical reason to suppose that one magmon should crystallize completely before the next magmon arrives, leading to a prima facie expectation that each magmon interacts with residual liquids left over from previous magmons.

In the idealized RMTX model of O'Neill & Jenner (2012) for the global array of magma chambers forming the oceanic crust, the [MgO] of the erupted basalts, sampled as pillow-rind glasses, reflects the fraction tapped (ϕ_T) to crystallized (ϕ_X) in each cycle, given the ol:plag:cpx proportions crystallized. The fractions refer to the amount of magma in the magma chamber after tapping. The average erupted [MgO] of ~7·6 wt % corresponds to $\phi_T = 0{\cdot}12$ and $\phi_X = 0{\cdot}51$, which would translate to 19% 'basalt' to 81% 'cumulate gabbro' in the oceanic crust. The model therefore accounts fairly well for the proportion of 'basalt' to 'gabbro' in the crust, at least as this proportionality is understood at present. The scarcity of evolved OFB compositions with [MgO] < 5 wt % is also explained, as such evolved compositions cannot be accessed by the RMTX process at steady state. Such evolved compositions would be expected where magma supply cannot keep up with eruption rates; for example, in the dying magma chambers as a consequence of a ridge jump (e.g. Sinton *et al.*, 1983). Similarly, highly evolved magmas are commonly described at propagating tips of rifts, such as those retrieved from the Galapagos, the Juan de Fuca Ridge and Deep Sea Drilling Project (DSDP) Site 32, in the eastern Pacific near California (Christie & Sinton, 1981; Sinton *et al.*, 1983). With increasing distance from the propagating tips of rifts, erupted compositions quickly approach those of 'normal' OFB compositions (Sinton *et al.*, 1983, figs 2 and 5), implying evolution of the systems towards the steady-state paradigm that we take as representing the stochastic processes of the global spreading system.

O'Neill & Jenner (2012) erroneously stated that steady state would not be obtained in their model at [MgO] > 8·6 wt % because $(\phi_T + \phi_X) \geq 1$, but, as Coogan & O'Hara (2015) pointed out, there is no such restriction implicit in the definitions of ϕ_T and ϕ_X, which are those of Albarède (1985), if the replenishment inflates the magma chamber before tapping. In principle, ϕ_T could become very large. For that reason, Coogan & O'Hara (2015) preferred to use a different basis for defining fractions tapped and crystallized (Φ_T and Φ_X; note the use of Φ rather than ϕ), referring the fractions to the amount in the magma chamber before tapping, such that $\Phi_T = \phi_T/(1+\phi_T)$ and $\Phi_X = \phi_X/(1+\phi_T)$. The two coordinate systems for the global ensemble of magma chambers of O'Neill & Jenner (2012) are shown in Fig. 1a. The model of O'Neill & Jenner (2012) assumes that mixing occurs before tapping (RMTX), whereas O'Hara's earlier models (O'Hara, 1977; O'Hara & Mathews, 1981) assumed that tapping preceded mixing after replenishment (i.e. the sequence RTMX). The latter option implies that the erupted basalts would indeed be cotectic liquids, not a mixture of the cotectic and replenishing liquid as in the RMTX sequence.

The global ensemble of steady-state RMTX magma chambers invoked by O'Neill & Jenner (2012) is a stochastic model addressing the average behaviour at the global scale. Individual volcanic centres along the mid-ocean ridge system operate with parameters whose values will be distributed about the average. Part of the variability of OFB compositions then reflects not only the distribution of these parameters (i.e. in ϕ_X:ϕ_T, or in proportions of olivine, clinopyroxene and plagioclase crystallizing, denoted hereafter f_{ol}:f_{cpx}:f_{plag}), but also the stochastic deviations from the idealized RMTX process itself. For example, rather than the perfect sequence of RTXRTXRTX... (mixing to be understood), with constant ϕ_X and ϕ_T at each cycle, real magma chambers may have ϕ_X and ϕ_T that vary between cycles, never reaching steady state, and tapping may sometimes follow rather than precede fractionation (RMXT rather than RMTX). The magma chambers may undergo several episodes of tapping between replenishment (RTXTXTXT...), which would produce a sequence of lavas related by SFX. And differentiation within flows after eruption (e.g. Rubin *et al.*, 2001) may be expected to proceed also by SFX. As noted by O'Neill & Jenner (2012), the global arrays of log [M] vs [MgO] is probably built up of short segments or chords of samples related by SFX stacked en echelon.

Other hypotheses for the incompatible element over-enrichment

Incompatible element over-enrichment is not uniquely a signature of RMTX processes, raising the question of whether other hypotheses could account for the geochemical observations. Coogan & O'Hara (2015) have shown that over-enrichments similar to those produced by the RMTX process could be engendered by the '*in situ* crystallization' equations of Langmuir (1989). In this hypothesis, crystallization in one part of the magma chamber traps melt interstitially; this melt evolves by further crystallization, until it is returned to mix in with the less evolved melt in the rest of the magma chamber, which is then erupted. In this scenario, the returning, more evolved melt would be denser (Fig. 1b), because, being more evolved, it is richer in Fe. A somewhat similar scenario was proposed by Lissenberg *et al.* (2013), which they labelled 'reactive porous flow'. An essential feature of either hypothesis is that the over-enrichment of incompatible trace elements is caused by more evolved, hence cooler melts, which, mainly because they are richer in Fe, are also denser; this raises the problem of how a denser melt or mush could rise to mix in with the less dense melt in the magma chamber. In contrast, in the RMTX model, it is the incoming parental melts that have the lower density, which is a prerequisite for mixing in a magma chamber (Sparks *et al.*, 1980; Turner & Campbell, 1986).

The compositions of melt inclusions may also discriminate between over-enrichment processes. The influx of cooler, evolved melt into the magma chamber containing melt that is already saturated in olivine, with or without plagioclase and clinopyroxene, might be expected to promote rapid crystallization of these phases, trapping the evolved melt as inclusions. Such inclusions seem to be rarely found: the literature on the melt inclusions in OFB phenocrysts (e.g. Kent, 2008) has emphasized the presence of compositions that are more primitive than the host magma, as required by RMTX models, not more evolved. By contrast, influx of hotter, more primitive melts into the magma chamber is likely to promote rapid olivine growth and trapping of primitive, highly variable melt compositions, which, indeed, are frequently observed (Coogan, 2014). There is little evidence to support the hypothesis that the olivine phenocrysts with melt inclusions of primitive composition are carried up from the mantle roots of the volcanic plumbing system: the relatively rapid diffusion of many trace elements through olivine precludes the survival of melt inclusions that are compositionally distinct from the host magma during reasonable transit times (Spandler *et al.*, 2007). Instead, the volatile contents of olivine-hosted inclusions are consistent with them being sampled from the pressure interval corresponding to the crust, often with the majority being trapped at shallow levels (Wanless *et al.*, 2015).

As contrary evidence, there is the frequent occurrence of olivine and plagioclase phenocrysts that are too primitive to be in equilibrium with their host magmas (e.g. Coogan, 2014; Coogan & O'Hara, 2015). Phenocrysts that are more evolved than their host melts should show signs of being resorbed, making them stand out during petrographic examination, but despite this are much less often described. Coogan & O'Hara (2015) used this observation to argue for the enriched-into-depleted scenario, whereas within the RMTX paradigm such crystals would indicate pre-magma-chamber

crystallization, or crystallization before mixing is complete.

Although chlorine was determined in only 105 of the OFB glass samples analysed by Jenner & O'Neill (2012), there are sufficient data to show that Cl abundances increase similarly with [MgO] to those of other incompatible trace elements, with similar slope (–0·21) and variability (23%). This similarity argues against significant contamination by seawater or hydrothermal brines, or assimilation of altered crust.

Constant (Sm + Gd)/Ti in OFB and its significance

A geochemical constraint on the over-enrichment process comes from the absence of an Fe–Ti oxide signature in OFB above ~5 wt % MgO. Plots of log [Ti] vs log [REE] in OFB have a slope of unity near Eu, establishing that Ti has the same incompatibility as Eu on average during OFB petrogenesis (e.g. Jenner & O'Neill, 2012*a*). To avoid the noise from the variable oxidation state of Eu, (Sm + Gd) can be used rather than Eu. Above ~5 wt % MgO, (Sm + Gd)/Ti is remarkably constant at 10^4(Sm + Gd)/Ti = 8·61 ± 0·47 (Fig. 2). The standard deviation of 5·4% is not much greater than analytical precision; this would be 3·7% if the analytical precision on each element were 3% (Jenner & O'Neill, 2012*b*). As there is no *a priori* reason to suppose that Ti falls exactly halfway between Sm and Gd in its incompatibility, a more general approach would be to consider the ratio (Sm + *n*Gd)/Ti, where *n* is a constant to be determined by optimization. We find *n* = 0·68, but the improvement as measured by the relative standard deviation is negligible, so we keep with the simpler ratio. There is one outlier at 6·2 wt % MgO, VG11242 from the Pacific–Antarctic ridge, which also has the highest Sm/Hf in the dataset, and relatively low P/Pr, so it seems an unusual sample.

Apart from this one sample, the constant (Sm + Gd)/Ti rules out a role for Fe–Ti oxides in the low-pressure evolution of OFB above ~5 wt % MgO, such as would be expected if the over-enrichment effect were due to the mixing back in of more evolved melts that had crystallized Fe–Ti oxides, or if there was contamination or other interaction with the gabbros of the lower oceanic crust, where Fe–Ti oxides are common (Coogan, 2014). The effect of Fe–Ti oxides on raising (Sm + Gd)/Ti ratios can be seen in back-arc basin basalts (Fig. 2b). This is not to say that highly evolved magmas do not infiltrate the lower crust, by such processes as the reactive porous flow described by Lissenberg *et al.* (2013) or other forms of mush–melt interactions [see Coogan (2014) for a summary of the evidence]. However, perhaps because of their high density, such melts do not mix with less evolved magma to influence the chemistry of erupted OFB, but instead solidify in the lower crust, giving rise to the metasomatized compositionally diverse lithologies whose occurrence is not disputed.

The remarkably constant (Sm + Gd)/Ti has further significance for the petrogenesis of OFB. The lack of change with MgO (Fig. 2a and b) implies that the bulk partitioning of (Sm + Gd) and Ti are both controlled by a single phase during partial crystallization, which is obviously clinopyroxene (Fig. 2c). In upper mantle peridotite, Sm and Gd are also mainly held in clinopyroxene, but Ti is more evenly distributed between clinopyroxene and orthopyroxene. For example, using the parameterization of $D_M^{cpx/opx}$ of Witt-Eickschen & O'Neill (2005, table 4), as a function of temperature and clinopyroxene composition at an assumed pressure of 15 kbar in spinel lherzolite xenoliths, values of $D_{Sm}^{cpx/opx}$ and $D_{Gd}^{cpx/opx}$ are between 10 and 20 at appropriate conditions for partial melting of spinel lherzolite, whereas $D_{Ti}^{cpx/opx}$ is only ~ 2. Experiments at 1300°C and 1 bar give $D_{Ti}^{cpx/melt}/D_{Ti}^{opx/melt} = 3·0 \pm 0·1$, but with different melt compositions for orthopyroxene and clinopyroxene (Mallmann & O'Neill, 2009). This means that the (Sm + Gd)/Ti of the melt decreases with the degree of partial melting as clinopyroxene is progressively melted out. The details depend on the partition coefficients, mineral modes and melting reactions, but only to second order, and a representative model calculation, presented in Fig. 2c, is typical. The constant (Sm + Gd)/Ti observed in OFB glasses is therefore evidence for a high and fairly uniform degree of partial melting at the global scale, of a source that has little dispersion in (Sm + Gd)/Ti.

VARIABILITY AND INCOMPATIBILITY

The variability [see equation (2)] of elements in global OFB correlates with their slopes, d(log[M])/d[MgO] (Fig. 3), demonstrating that variability increases with incompatibility. An exception to this rule are the variabilities of the most incompatible elements (here, Ba, Rb, Cs, Th, U, Nb, Ta and W), which have been referred to as the very incompatible elements (VICE) (Hofmann & Jochum, 1996), which differ in variability but share a common slope. For other incompatible trace elements, the trend of variability against slope shown in Fig. 3 leads to a natural classification, as follows. Highly incompatible elements (HICE) cover the range of the light rare earth elements (LREE) from La to Gd, which may be extended to include K, an element that otherwise falls into a large gap between the VICE and La. The HICE show an increase of variability with decreasing slope. Moderately incompatible elements (MICE) comprise the rest of the REE from Gd to Lu, plus Y, and have nearly the same variability, independent of slope. The lightly incompatible elements (LICE), which are the elements less incompatible than Lu, the heaviest REE, show lower variabilities than the MICE. With the significant exception of phosphorus (a HICE), all the VICE, HICE and MICE shown in Fig. 3 are preferentially held in clinopyroxene over orthopyroxene in spinel lherzolite, with negligible amounts in olivine or spinel. This gives the constant P/Nd in OFB a considerable significance in understanding OFB petrogenesis because P is the only

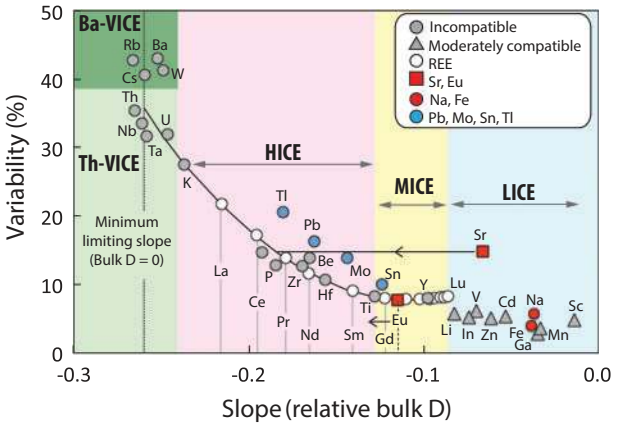

Fig. 3. Slopes (d(log[M])/d[MgO]) vs variability [see equation (2)] for the OFB data of Jenner & O'Neill (2012*a*). Elements are grouped according to their partitioning behaviour during OFB differentiation as follows: very incompatible elements (VICE); highly incompatible elements (HICE); mildly incompatible elements (MICE); lightly incompatible elements (LICE). The VICE group can be divided into two sub-groups: Ba-VICE, including Rb, Cs and W, and Th-VICE, including Nb, Ta and perhaps U, on account of the anomalously high variabilities of the Ba-VICE compared with the trend through the HICE and the Th-VICE group. The cause of the notably lower variability for the LICE compared with the MICE and the higher variability of the Ba-VICE compared with the Th-VICE and Pb compared with Nd remains enigmatic, but might relate to differences in the relative mobility of elements during recycling of the subducted slabs into the mantle since the onset of subduction. Sr shows anomalously high variability compared with elements with comparable slopes, which can be attributed to the role of plagioclase during low-pressure differentiation of OFB.

element among the VICE, HICE or MICE that is preferentially held in olivine (Mallmann & O'Neill, 2009).

When extrapolated back to parental OFB compositions at ~10·5 wt % [MgO], the average concentrations of the refractory lithophile elements among the VICE and HICE are depleted, relative to their expected values, from chondritic ratios with the MICE [i.e. heavy REE (HREE) and Y], and the extent of the depletion correlates well with their slopes and variabilities (see O'Neill & Jenner, 2012, fig. 3). All the MICE are refractory lithophile elements, but Sc is the only such among the LICE. The VICE and HICE depletion has traditionally been explained by their extraction from the OFB source mantle into the continental crust (e.g. Hofmann, 1988), but some fraction of the Bulk Silicate Earth's complement of these elements may also have been lost by collisional erosion of early formed crust during Earth's accretion (O'Neill & Palme, 2008).

The common slope of the VICE results in ratios such as Ba/Ta, Ba/Th, Ba/Rb and Ba/W remaining constant with decreasing MgO (Fig. 4a and b). This observation, together with the large range in variabilities of the VICE (Fig. 3), was interpreted by O'Neill & Jenner (2012) as reflecting bulk D_M of zero during their low-pressure evolution. Therefore, their variabilities, which range from 32 to 43% (Fig. 3), are mainly inherited from the parental melts. The VICE divide into two subgroups, one comprising Ba, Rb, Cs and W with higher variabilities, the other Th, U, Nb and Ta with lower variabilities that fall on the extension of the curve drawn through the REE. Although U is customarily compared with Th or Nb in basalt geochemistry, it consistently seems to be resolvably less incompatible than the other VICE in large datasets of OFB (e.g. Sun *et al.*, 2008; O'Neill & Jenner, 2012). As for their chemical properties, the Ba-VICE tend to be water-soluble, the Th-VICE are traditionally regarded as not.

Ba/Ta and Ba/Th increase with increasing [Ba], whereas Ba/Rb and Ba/W remain constant with increasing [Ba] (Fig. 4c). With the exception of Ba/W, comparable trends are also observed using the OFB dataset of Gale *et al.* (2013) (Fig. 4d). These differences reflect variability in parental OFB compositions. Massive fractionations of the VICE during partial melting are implausible, because they are inconsistent with the evidence from the less incompatible HICE, MICE and LICE; for example, the constant (Sm + Gd)/Ti (Fig. 2). A discussion of the REE evidence on this issue has been given by O'Neill (2016). The variability of the VICE in parental OFB magmas must simply be inherited from the variability of their source.

As is well known, there are distinctive features in OFB in the ratios among the four refractory lithophile elements (RLE) comprising the Th-VICE subgroup (namely Th, Nb, Ta and here also including U), exemplified by the non-chondritic ratios Th/U, Nb/U and Nb/Ta, which have become iconic in mantle geochemistry (Fig. 5). The relative depletion of these elements increases in the order Th > U > Nb > Ta (e.g. Hofmann *et al.*, 1986; Campbell, 2003), but there are different explanations for the depletions. The depletion of Nb relative to its chemically similar companion in the periodic table, Ta, with Nb/Ta ~ 15% below chondritic, has been ascribed to partitioning of some Nb into the Earth's core in the earliest stages of the Earth's history (Wade & Wood, 2001); the low Nb/Ta is therefore thought to be characteristic of the Bulk Silicate Earth, rather than just the OFB source mantle.

Despite this Nb depletion, Nb/U in OFB is superchondritic, which is complementary to the subchondritic Nb/U of the continental crust (e.g. Rudnick & Gao, 2003, and references therein). The explanation lies in the preferential retention of Nb and Ta in the subducting slab (oceanic crust and overlying sediments) relative to the other VICE during convergent margin magmatism, with the bulk of the continental crust formed via this magmatism (e.g. Elliott *et al.*, 1997; Rudnick & Gao, 2003, and references therein; Pearce *et al.*, 2005; König *et al.*, 2008; Bebout, 2014). This implies that the timescale over which the characteristic Nb/U of the OFB source is produced is related to that over which the continental crust forms—a different timescale from that responsible for the low Nb/Ta ratio. Because of the aforementioned depletion of Nb by partitioning into the core, and the possibility of enhanced U recycling in the Phanerozoic addressed next, the Nb/U story would be better told through Ta/Th.

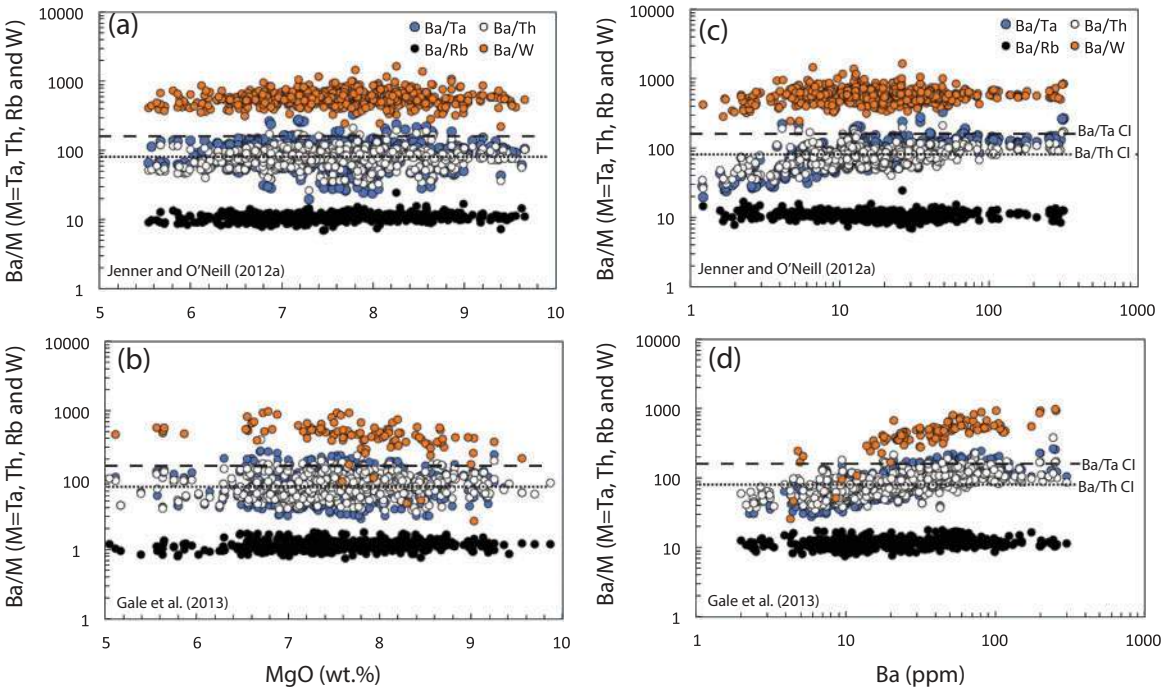

Fig. 4. Variation of VICE inter-element ratios versus MgO (a, b) and Ba (c, d) using the OFB datasets of Jenner & O'Neill (2012*a*) and Gale *et al.* (2013) and compared with Cl-chondritic ratios (Palme *et al.*, 2014) for the refractory lithophile elements. Both datasets show constant VICE inter-element ratios when plotted versus [MgO], because each element has a similar slope (compatibility) during differentiation of OFB (see Fig. 3). Inter-element ratios within the Ba-VICE or the Th-VICE subgroups (e.g. Ba/Rb and Ba/W or Th/Ta) are constant with increasing [Ba], whereas ratios between elements in the different VICE subgroups (e.g. Ba/Th and Ba/Ta) show an increase with increasing [Ba], which is attributed to variabilities in parental OFB melts and, thus, the OFB-source mantle. Ba/Ta and Ba/Th for OFB [using the datasets of Jenner & O'Neill (2012*a*)] are in the range of 20–327 (average = 93 ± 39) and 26–209 (average = 83 ± 26), respectively. The average Ba/Th of OFB is comparable with that of Cl-chondrites (Ba/Th = 81), whereas the average Ba/Ta of OFB is significantly sub-chondritic (Ba/Ta of 161), which could be balanced by a higher Ba/Ta in the continental crust (Ba/Ta = 651). The same relationships are shown by the dataset of Gale *et al.* (2013), except for Ba/W versus Ba.

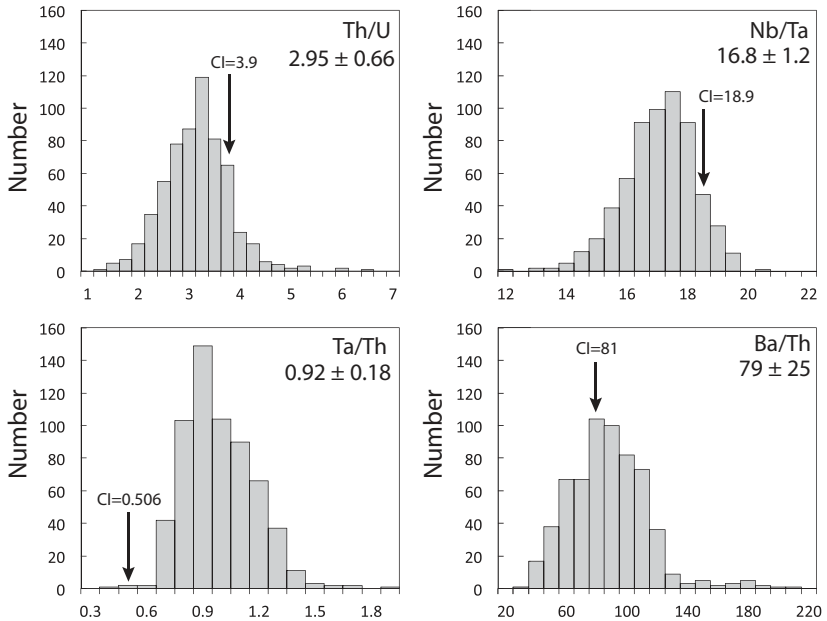

Fig. 5. Histograms of ratios among some VICE refractory lithophile elements from the global dataset of Jenner & O'Neill (2012*a*). Cl-chondritic ratios from Palme *et al.* (2014).

The third of the iconic non-chondritic ratios among the Th-VICE is Th/U, which has been much studied because of the extra information that Th–U–Pb isotope systematics can give, including the time dimension. The Th/U ratio in OFB is 2·9 (Fig. 5) compared with the chondritic ratio of 3·9 (Blichert-Toft *et al.*, 2010). The Pb isotopic compositions of OFB record a long-term time-integrated chondritic Th/U ratio. One interpretation of

this observation (known as the 'second Pb paradox', or 'kappa conundrum') is that the Pb is recycled from the continental crust, which does have approximately chondritic Th/U (e.g. Chauvel *et al.*, 1995). Alternatively, Th/U could be low because of the preferential recycling of oxidized U (as U^{6+}), which is soluble in fluids, back into the mantle compared with insoluble Th (e.g. Elliott *et al.*, 1997; Collerson & Kamber, 1999), a view that has recently received support from studies of the fractionation of U isotopes (Andersen *et al.*, 2015). This process becomes possible only after the Great Oxidation Event at ~2·3 Ga, or, more likely, after full ocean oxidation at 0·6 Ga (Andersen *et al.*, 2015). But preferential recycling of water-soluble VICE should elevate Ba/Th (e.g. Turner *et al.*, 1997; Pearce *et al.*, 2005). Association of water-soluble U^{6+} and Ba would manifest itself in a negative correlation between Ba/Th and Nb/U, of which there is no sign (the global dataset has a small positive correlation). Other evidence that U is associated with the Th-VICE and not the Ba-VICE will be presented below. The geometric mean Ba/Th, corresponding to its integrated value over global OFB, is chondritic (Fig. 5), but the variation of Ba/Th about this mean is not random. Rather, the change of Ba/Th with [Ba] (Fig. 4) crosses the chondritic ratio, showing that the VICE-enriched OFB source has a higher Ba/Th.

The variabilities of the VICE present something of an enigma. The absolute abundances of the VICE are extremely dispersed, covering two-and-a-half orders of magnitude in OFB (Fig. 4), showing that the OFB source mantle is very inhomogeneous in these elements. Compositionally inhomogeneous mantle implies poorly mixed mantle. Yet the ratios among these elements are not the chondritic ratios expected of 'primitive mantle', but attest to the net result of several different processes, including formation of the continental crust (Ta/Th, Nb/U), and recycling of the oceanic crust and overlying sediments (Th/U). Moreover, such processes have operated over different timescales. The enigma is the relative constancy of these fractionated ratios (the best example is Ta/Th), which would seem to require good mixing.

The anomalous variability of Sr

Significantly anomalous on the variability vs slope plot (Fig. 3) is Sr, whose position on the plot could be taken as being either above the trend defined by the other elements (higher variability at a given slope), or, alternatively, to the right of the curve (less negative slope at a given variability). The latter option is suggested by the behavior of Eu. Plotting the slopes and the variabilities of all the REE against atomic number reveals that it is mainly the slope of Eu that is anomalous—it is less negative than interpolation between Sm and Gd would suggest. The less negative slope is due to its compatibility in plagioclase, which also explains the Sr anomaly. Shifting the position of Sr to the left in Fig. 3 to fall on the variability vs slope curve would put its incompatibility similar to Pr, a LREE. That the Sr anomaly is not caused by interaction with seawater is shown by the lack of correlation of Sr/Pr with Cl in the datasets of Jenner & O'Neill (2012*a*) and Le Voyer *et al.* (2015).

Similarly plotting off the main trend in Fig. 3 are Pb, Tl, Mo and Sn. Given the very low levels of these elements, especially Tl, analytical uncertainty may contribute. For Pb and Tl, compatibility in plagioclase may be a factor, as for Sr. Alternatively, these elements are somewhat chalcophile, with Pb having $D^{\text{sulfide melt/silicate melt}}$ of 57 (Patten *et al.*, 2013), which may result in a less negative slope because of partitioning into immiscible sulfide melt. The more incompatible the element in silicates, the more noticeable the effect on the slope of a small fraction of immiscible sulfide in the cotectic assemblage, for a given $D^{\text{sulfide melt/silicate melt}}$.

The structure of incompatible element variability in global OFB

Na, P, K and Ti have slopes (Fig. 3) spanning from the LICE (Na) and MICE (Ti) to the HICE (P and K, which is almost a VICE). Detailed scrutiny of the variabilities of these elements is made possible by the large amount of data available in the Smithsonian Abyssal Volcanic Glass Data File (Melson *et al.*, 2002), which reveals a remarkable structure to their variabilities as a function of low-pressure evolution, as monitored by [MgO] (Figs 6 and 7). Binning the data into ranges of [MgO] shows that all four elements approximate a log-normal distribution in the more primitive magmas, and this log-normal distribution is maintained in the bins of decreasing [MgO] (Fig. 6). A modest exception is the distribution of Ti, which develops a tail to low Ti concentrations, but it should be noted that this tail comprises only ~5% of the glasses in the 5·5–6·5 wt % MgO bin (Fig. 6b).

Much attention has been given to incompatible-element enriched OFB (so-called E-MORB), since early studies claimed an association between incompatible element enrichment and the Iceland plume (Schilling, 1973) or the Azores plume (Schilling, 1975); however, it is now known that these basalts occur everywhere in the ridge system (e.g. Donnelly *et al.*, 2004; Brandl *et al.*, 2016; O'Neill, 2016). With the exception of the low-Ti OFB, the important observation here is that the enriched OFB are part of the same unimodal log-normal distribution as depleted OFB (Fig. 6; see also fig. 4c of Jenner & O'Neill, 2012*a*). If enriched OFB were a signature of a different process, such as being related to thermal plumes, we would expect a bimodal distribution.

We cannot at present test whether the low-Ti OFB are due to mixing back in of evolved melts that have undergone Fe–Ti oxide crystallization, or the other possibilities discussed in the (Sm + Gd)/Ti section, as there are no REE data in the Smithsonian database, and there is only one example in the Jenner & O'Neill (2012*a*) subset at >5·5 wt % MgO (Fig. 2). The existence of anomalously low [Ti] samples among the more evolved OFB

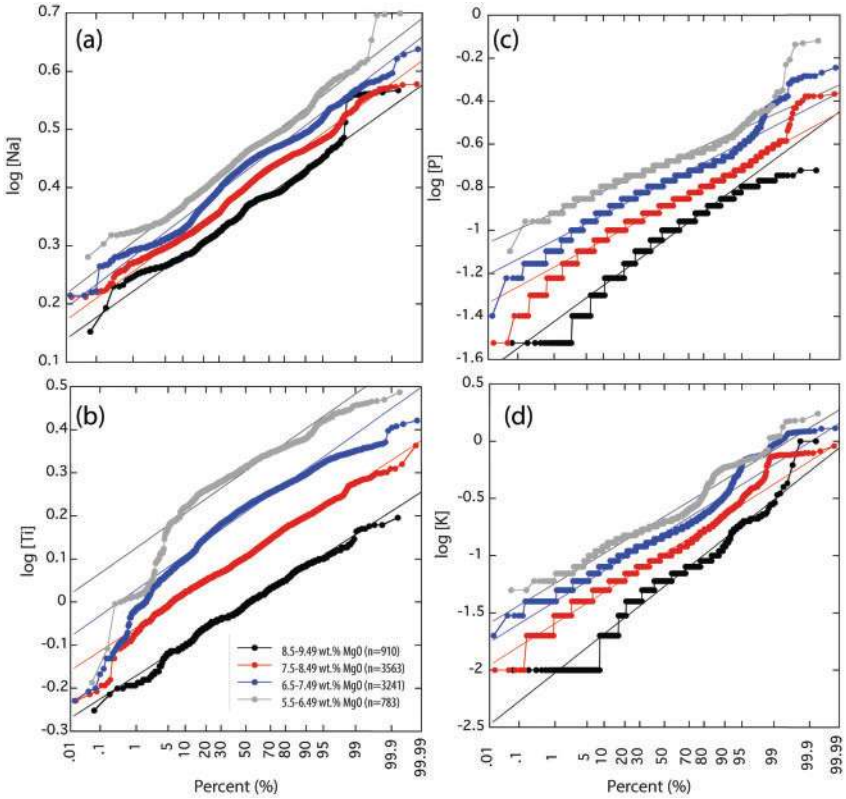

Fig. 6. Cumulative probability (logarithmic scales) for Na, Ti, P and K, binned by [MgO], showing that the distribution of these elements is log-normal in all bins, except for Ti in the < 6·5 wt % MgO bin, which shows a tail at low [Ti]. However, this tail consists of only < 5% of the population in this bin, hence < 0·5% of all samples.

glasses is a new observation, as far as we know, which deserves further investigation.

The variabilities of Na and Ti (LICE and MICE) increase with decreasing [MgO], hence with increasing evolution (Fig. 7). On the other hand, those of K and P (HICE) remain constant within uncertainty up to ~8·5 wt % MgO, but the higher bins have larger variabilities. The increased variability in these less evolved melts may reflect inefficient mixing of compositionally variable components of the parental melts (e.g. Shorttle, 2015). Alternatively, it may only reflect increasing analytical imprecision, as the typical abundances of K and P trend towards the limit of detection of the electron microprobe (EMP). This can be demonstrated by comparing the Smithsonian EMP data with more precise analyses obtained using laser ablation inductively coupled plasma mass spectrometry (LA-ICP-MS) analysis (Fig. 7e–h). The pixilation of the data for K and P apparent in Fig. 6c and d is another manifestation of low abundances relative to detection limits. The confidence limits (95%) of the variabilities decrease slowly as the number of data increase (Fig. 7), so it is necessary to have the large numbers of data in the Smithsonian Abyssal Volcanic Glass Data File to allow the increase of the variability of Na and Ti with decreasing [MgO] to be observed with confidence. We now explore the implications of this observation.

Partitioning of variability: parental magmas versus crustal evolution

Most of the processes hypothesized for the low-pressure evolution of a magma relate the concentration of an incompatible trace element [M] to its concentration in the parental melt, $[M]_o$, through an equation that has the general form

$$[M] = [M]_o f(x_1, x_2, \ldots, x_n) \quad (3)$$

where x_1, x_2,..., x_n are the variables of the model. For SFX, for example, the variables are the bulk mineral–melt partition coefficient, D_M, and the degree of crystallization F, and the equation is

$$[M] = [M]_o F^{(D_M - 1)}. \quad (4)$$

Similarly for the idealized RMTX process, the process is described by

$$[M] = [M]_o(\phi_X + \phi_T)/[1 + \phi_T - (1 - \phi_X)^{D_M}] \quad (5)$$

(formulation of Albarède, 1985). Then by propagation of errors

$$\sigma([M])^2 \approx \sigma([M]_o)^2 f(x_1, x_2, \ldots, x_n)^2 + [M]_o{}^2 \sum_n \left[\left(\frac{df(x_1, x_2, \ldots, x_n)}{dx_n} \right)^2 \sigma(x_n)^2 \right]. \quad (6)$$

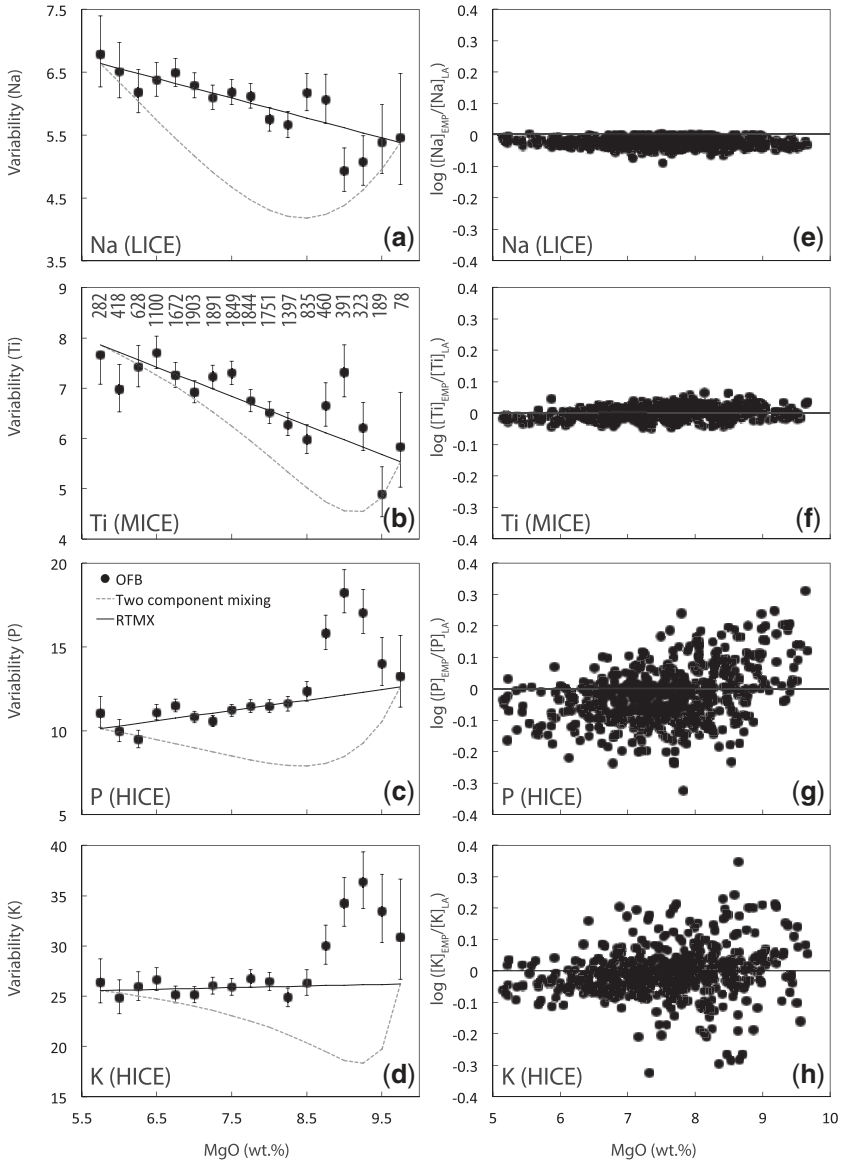

Fig. 7. (a–d) Variabilities of Na, Ti, P and K from the Smithsonian Abyssal Volcanic Glass Database (Melson *et al.*, 2002) for samples with [MgO] > 5·5 wt % ($n = 8575$) in overlapping bins of 0·5 wt % MgO. The error bars show the 95% confidence intervals. The continuous line shows the standard deviations for the modelling presented here [equation (6)]. The dashed curves show the standard deviations for modelling two-component mixing between a high [MgO] melt (10 wt % MgO) and a low [MgO] melt (5 wt % MgO) with standard deviations equal to those observed in the real populations. It should be noted that mixing produces a minimum at intermediate [MgO]. The variabilities of Na and Ti increase with decreasing [MgO], whereas P and K remain approximately constant except for an increase in variability at high MgO (>8·5 wt % MgO). This is probably due to analytical uncertainty as these elements approach the limits of detection of the electron microprobe (EMP). The better determined Na and Ti do not show this effect. (e–h) The additional uncertainty in EMP determination of P and K is demonstrated by comparing the Smithsonian data (Melson, 2002) with the more precise analyses undertaken using LA-ICP-MS presented by Jenner & O'Neill (2012 *a*) on a subset of samples.

This partitions the distribution of M into two contributions: a contribution inherited from the distribution in the parental melts, with standard deviation $\sigma([M]_o)$, and a contribution that can be attributed to low-pressure evolution, given by the second term on the right-hand side. This term could potentially be complex, not least because the parameters of the model are not necessarily independently variable, introducing off-diagonal terms in a variance–covariance matrix. But one extreme would be the case of a VICE element undergoing simple fractional crystallization, where the concentration of the element is almost independent of the parameters of the process, such that the second term on the right-hand side of equation (6) would be small. If we take it as zero, then equation (6) would reduce to

$$\sigma([M]) = f(x_1, x_2, ..., x_n)\sigma([M]_o) = \sigma([M]_o)[\overline{M}]/[M]_o \quad (7)$$

where $[\overline{M}]$ is the mean of the distribution of [M] at the stage of evolution given by $f(x_1, x_2, \ldots, x_n)$. This shows that $\sigma([M])$ increases with increasing $[\overline{M}]/[M]_o$, but the

variability as defined by equation (2), obtained from equation (7) by substituting $\sigma(\log[M]) = \sigma([M])/2{\cdot}303[M]$, is constant:

$$\sigma(\log\,[M]) = \sigma(\log\,[M]_o). \quad (8)$$

The increasing variability of Na and Ti with decreasing [MgO] shown in Fig. 7 then shows that the low-pressure evolution [the second term on the right-hand side of equation (6)] is indeed contributing to the variability. Extrapolation of the trends in Fig. 7 to the presumed parental composition at $[MgO]_o = 10{\cdot}4$ wt% gives variabilities of Na and Ti of 0·050 and 0·055 respectively. These variabilities increase to 0·060 and 0·068, respectively at 7·6 wt% MgO, the average [MgO] of OFB according to Gale *et al.* (2013). Applying these observations to equation (6) then shows that for average OFB at 7·6 wt % MgO, the variability owing to low-pressure evolution for Na is $(0{\cdot}06^2 - 0{\cdot}050^2)^{1/2}$, or 0·033, or about 45%. For Ti, this value is 0·040, or about 42%. Conversely, for the more incompatible P and K, any variability developing during crustal evolution is obscured by the large variability inherited from the parental magmas.

The changes of $\sigma(\log[Na])$ and $\sigma(\log[Ti])$ with [MgO] calculated from the propagation of errors for two-component mixing between the populations of Na and Ti in the highest and lowest MgO bins are also plotted in Fig. 7, from which it may be seen that two-component mixing would produce a minimum in the variability vs [MgO] plots, which is not observed. This is evidence that the global trends vs [MgO] in OFB are not produced by two-component mixing of an MgO-rich component (a peridotite-derived partial melt) with an independently derived MgO-poor component, such as a pyroxenite melt.

CORRELATION COEFFICIENTS

The correlations between the variabilities of different elements provide the path to a better understanding of their causes. The variability is composed of the residuals, $\log[M] - \log[M]_{calc}$ (alternatively written $\log[M]/[M]_{calc}$), and the covariances between the residuals of two elements A and B is

$$\mathrm{covar}(A,B) = 1/n \sum \log([A]/[A]_{calc})\log([B]/[B]_{calc}). \quad (9)$$

To compare elements that differ greatly in their variabilities (e.g. the VICE with the LICE; see Fig. 3), it is advantageous to normalize the covariances to pairwise correlation coefficients:

$$\mathrm{corr}(A,B) = \frac{1}{n}\sum \frac{\log\,([A]/[A]_{calc})\ \log\,([B]/[B]_{calc})}{\sigma(\log\,[A])\sigma(\log\,[B])}. \quad (10)$$

The matrix of correlation coefficients from the database of Jenner & O'Neill (2012*a*) for samples with >5·5 wt % MgO is given in Supplementary Table 1 (supplementary data are available for downloading at http://www.petrology.oxfordjournals.org). All the VICE are highly correlated with each other [corr(A,B) ≫ 0·9], as already commented in reference to their relatively constant ratios. Even the correlations between members of the two different subgroups of VICE are high, with, for example, corr(Ba,Th) and corr(Ba,Nb) at 0·96 and 0·94 respectively.

The relationship between pairwise correlation coefficients, corr(A,B) and the absolute differences in slopes, abs[slope(A) – slope(B)], representing differences in incompatibilities, is shown in Fig. 8 for selected element pairs, including the suite of REE. Generally speaking, there is a strong negative correlation between corr(A,B) and the differences in slopes, exemplified by the REE. Particularly noteworthy are the high values of corr(A,B), often approaching unity, between elements with similar slopes but widely different chemical properties. One example that we have already discussed is (Sm + Gd)/Ti, but of great significance is P/Nd (or, slightly better, P/Pr), with correlation coefficients of 0·95. Phosphorus has a valence state of 5 + and has the unique property among VICE, HICE or MICE of favouring olivine over pyroxenes (O'Neill & Mallmann, 2007; Mallmann *et al.*, 2009), whereas Pr or Nd form 3 + cations that substitute into clinopyroxene. The constant P/Nd ratio in OFB provides a stringent test of petrogenetic hypotheses on the possible contribution of olivine-poor lithologies to basaltic melts (O'Neill & Mallmann, 2007). Similarly, Ti is much less incompatible in carbonatitic melts relative to the REE than in silicate melts (e.g. Dasgupta *et al.*, 2009), which, in light of the constant (Sm + Gd)/Ti (Fig. 2) and high corr(A,B) of Ti with Sm and Gd of 0·96 and 0·93, respectively (Supplementary Data Table 1), rules out significant contributions of carbonatitic melts to the incompatible trace element inventory of OFB, or carbonatitic metasomatism contributing to the variability of the OFB source.

Certain element pairs are inconsistent with the trend shown in Fig. 8. As already noted, Sr has an anomalous slope relative to Nd, and this manifests itself on this diagram by corr(Sr,Nd) plotting well off the trend as established by the inter-REE correlation coefficients. Also clearly anomalous is corr(Na,Fe). These two elements have identical slopes but their pairwise correlation coefficient is negative (i.e. they are anti-correlated).

In a series of benchmark papers, Klein & Langmuir (1987) and Langmuir *et al.* (1992) attributed variations in Na and Fe of OFB to differences in depth and extent of melting of the source region, respectively. In Fig. 9 we show the pairwise correlation coefficients of the REE with Na, Fe and the other LICE. The pairwise correlation coefficients of LICE that are mainly held in clinopyroxene (e.g. V and Sc) share a similar pattern, in which corr(M,REE) increases with decreasing atomic number of the REE element, but with a dip at corr(Fe,Eu). Lithium, which is more evenly distributed

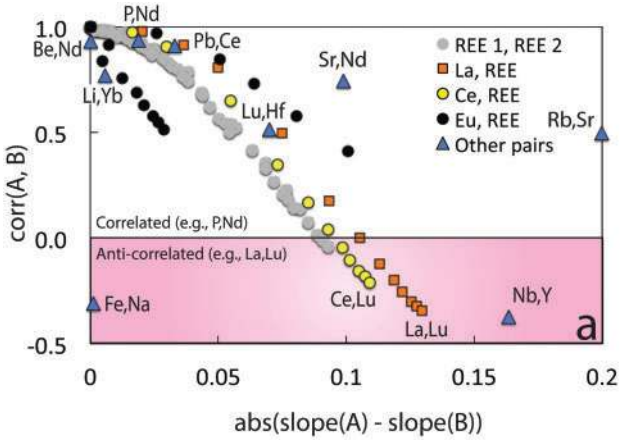

Fig. 8. The relationship between pairwise correlation coefficients of residuals of two elements A and B [corr(A,B); see equation (10)] versus abs[slope(A) – slope(B)] (i.e. the difference in slopes between elements A and B, representing differences in compatibilities) for selected element pairs, from average global trends (O'Neill & Jenner, 2012). Negative corr(A,B) are referred to as 'anti-correlated' [e.g. corr(Fe,Na), corr(Ce,Lu) and corr(Nb,Y)]. Values are given in Supplementary Data Table 1, including elements not plotted here [e.g. all the VICE are highly correlated with each other and have corr(A,B) > 0·9]. Generally corr(A,B) varies inversely and systematically with abs[slope(A) – slope(B)], as shown, for example, by REE pairs, but notable exceptions are corr(Sr,Nd), corr(Rb,Sr) and corr(Fe,Na).

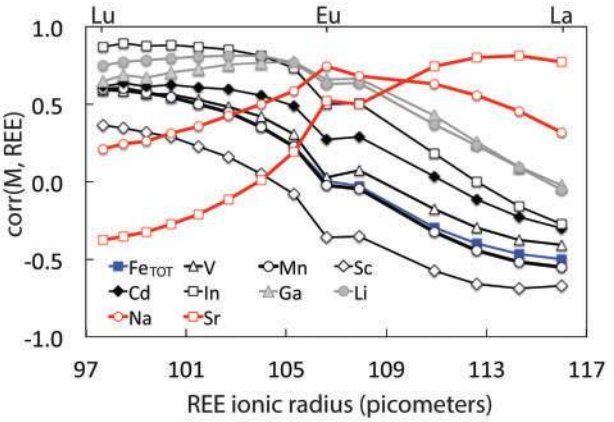

Fig. 9. The relationship between pairwise correlation coefficients of residuals of two elements A and B [i.e. corr(A,B); see equation (10)] from average global trends (O'Neill & Jenner, 2012) between LICE (Sc, V, In, Ga, Sr, Li, Cd, Na, Mn and Fe_{TOT}) and REE, plotted against the ionic radius of the REE. Such a plot reveals patterns in the variabilities around the main trend, caused by similarities and differences in the partition coefficients between phases, hence the nature of the phases. The difference in corr(Na, REE) and corr(Sr, REE) from corr(M, REE) for the other LICE with similar slopes, d(log[M])/d[MgO], argues for control of Na and Sr variability by crustal processes involving plagioclase rather than mantle processes in which plagioclase is not present. Similarly, the coherence between V and Fe variabilities argues for control by crustal processes in which clinopyroxene is the dominant host of both, rather than the mantle where V is hosted in clinopyroxene but Fe is dominated by olivine. The similarities in pattern between Ga and Li indicate that the distribution of these two elements among the cotectic phases is similar. The values of corr(Mn,REE) are almost identical to those of corr(Fe_{TOT},REE), showing that the variability of FeO_{TOT} is like that of a trace element in global OFB.

among the three cotectic phases (olivine, clinopyroxene and plagioclase) has a similar pattern to the clinopyroxene-hosted elements, except a slight decrease in corr(Li,REE) from the middle REE (MREE) to the heavy REE (HREE), which is also observed for corr(Ga,REE). The values of corr(Fe,REE) are strikingly similar to those of corr(V,REE) and corr(Sc,REE), implying that the variabilities of Fe, Sc and V are controlled by the same factor, which we suggest is the ratio of clinopyroxene + olivine to plagioclase during crystallization, and not the effects of partial melting (either the degree of melting or source lithology), where varying proportions of olivine to clinopyroxene should influence the variability of Fe differently from those of V and Sc. By contrast, values of corr(Na,REE) show the opposite trend with a rise at corr(Na,Eu), which is also the case for corr(Sr,REE). This is more evidence that the anti-correlation of Na and Fe reflects the proportion of plagioclase versus clinopyroxene and/or olivine in the crystallization products of low-temperature evolution in the magma chamber (f_{ol}:f_{cpx}:f_{plag}), rather than being an effect of partial melting.

Principal component analysis

To visualize the multi-dimensional structure of the correlation coefficients better, we examine the matrix of correlation coefficients by principal component analysis (PCA). The procedure is as follows. Let the matrix of the standardized residuals of the selected trace elements M, $\log([M]/[M]_{calc})/\sigma(\log[M])$, be called $\overline{\mathbf{M}}$. The reason for standardizing the residuals by normalizing to $\sigma(\log[M])$ is to give equal weight to elements of different variabilities, otherwise the analysis would be dominated by the VICE. The only difference from the usual application of PCA is that we centre the data according to equation (1), the average at a particular [MgO], rather than to the simple average. The matrix of correlation coefficients (see Supplementary Data Table 1) is then $\overline{\mathbf{M}}^{\mathbf{T}}\overline{\mathbf{M}}$, which is a symmetrical matrix with dimensions $n \times n$, where n is the number of trace elements being considered (here, $n = 45$; see below). The singular value decomposition of the correlation matrix re-expresses it as $\overline{\mathbf{M}}^{\mathbf{T}}\overline{\mathbf{M}} = \mathbf{VSV}^{\mathbf{T}}$, where $\mathbf{V}$ is an $n \times n$ matrix consisting of the n columns of eigenvectors, $\mathbf{V_1}$, $\mathbf{V_2}$,..., $\mathbf{V_n}$, and $\mathbf{S}$ is a diagonal matrix whose entries are the eigenvalues, λ_1, λ_2,..., λ_n, which are the correlations of the data expressed by the new variables, the eigenvectors. Because the data are standardized, $\sum\lambda_n = n$ (i.e. 45).

We use all the samples from the database of Jenner & O'Neill (2012 *a*) with [MgO] > 5·5 wt % (597 samples), and include all the elements analysed in that study, except for those excluded for the following reasons (some for more than one reason).

1. Major elements (Mg, Al, Si and Ca), as these are buffered by the cotectic assemblage, and their correlations include a substantial tendency towards

negative correlations induced by the closure problem (analyses summing to 100%), but we do include Na and Fe, which act as trace elements during low-pressure processes (e.g. Na acts like Sr and Fe acts like V; Figs 3 and 9). Additionally, we use [MgO] as the variable monitoring the extent of crustal evolution, and accordingly it is included implicitly in the definition of variability, albeit in a different way.

2. Ni, Cr and Ge: these are compatible elements whose abundances are controlled by well-known partitioning characteristics specific to the element, so their variability does not correlate with those of other elements. Ni is controlled by olivine, Cr by Cr-spinel and Ge follows Si.
3. Highly chalcophile elements (S, Se, Cu, Ag and Bi), whose crustal evolution is dominated by sulfide crystallization (also Re, Pt and Au).
4. Elements not analysed in a significant percentage of the samples (S, Cl, Re, Pt, Au, As and Sb). For Na and Fe, EMP analysis values were used in preference to the LA-ICP-MS values, because LA-ICP-MS analyses for Na and Fe were not undertaken for all samples.
5. Elements with many samples near the limits of detection (Ag, Se, Sb, Re, Pt, Au, Bi), where the variability is dominated by analytical uncertainty.

This leaves 45 elements. The eigenvalues and eigenvectors from the PCA are given in Supplementary Data Table 2.

The eigenvectors are the 'principal components' but 'component' is a misleading designation, particularly in the context of geochemistry. It was introduced by Hotelling (1933) because of 'the conflicting usage attaching to the word "factor" in mathematics', which could hardly be more ironic given the conflicting usage attached to 'component' in geochemistry (see also Stracke, 2012). Rather than as 'components', it is appropriate to think of the eigenvectors as 'associations of variance', or here, 'associations of variability'. In the present context, the eigenvectors reflect how the elements behave at the intersection of their chemical properties with the relevant geological processes operating on those properties.

The proportion of the standardized variance (or here, variability) of an element, M, accounted for by each eigenvector, $\mathbf{V_n}$, is $(a_{V_n,M})^2\lambda_n$, where $a_{V_n,M}$ is the entry in $\mathbf{V_n}$ corresponding to M, and λ_n is the eigenvalue. The sum over all n eigenvectors, $\sum_n (a_{V_n,M})^2\lambda_n$, is unity for each M. Only two eigenvectors, $\mathbf{V_1}$ and $\mathbf{V_2}$, account for 81% of the total standardized variability (Supplementary Data Table 2), and these are approximately equal at 44% and 37%, respectively. This result depends on the trace elements selected, and to that extent is subjective, but it is remarkable that so much of the variability of incompatible trace elements in global OFB should depend on just two factors, and that these two factors are of more-or-less equal importance. The next two eigenvectors ($\mathbf{V_3}$ and $\mathbf{V_4}$) account for 8% and 2%, respectively, of the variability (95% of the total variability is accounted for by $\mathbf{V_1}$ to $\mathbf{V_7}$).

The contributions from each of the first three eigenvectors to each M are plotted against the slopes of log [M] vs [MgO] in Fig. 10. Because the entries appear as squared terms in these contributions, information is lost as to whether their values were positive or negative. We have therefore arranged these plots to distinguish between positive entries and negative entries (upper and lower panels of Fig. 10, respectively), which helps bring out the structure of the eigenvectors.

For most of the incompatible trace elements (including those forming the familiar set that appears in 'spider diagrams'), these first two eigenvectors account for >90% of their variabilities (e.g. 92% of K variability is accounted for by $\mathbf{V_1}$ and 98% of Gd variability is accounted for by $\mathbf{V_2}$; Supplementary Data Table 2). Much of the total variability missing from these two eigenvectors comes from the LICE and the HICE, which appear in $\mathbf{V_3}$ (Fig. 10). An eigenvector could be dominated by a single element if the element has unique chemical properties among the elements analysed during OFB petrogenesis, or if a significant part of its variability is due to analytical uncertainty not correlated with the analytical uncertainty of other elements, which would be expected for an element near its limit of detection. This latter factor is not a credible explanation for Na (26% variability in $\mathbf{V_6}$), nor Sc (14% variability in $\mathbf{V_7}$), as both of these elements are extremely well determined. For Na, there is also the security that it was analysed by two methods, EMP analysis and LA-ICP-MS, with good agreement (Jenner & O'Neill, 2012*a*, 2012*b*). Curiously, Li, Ga and Co make a joint appearance in $\mathbf{V_4}$, which contains 18%, 15% and 12% of their variabilities, respectively. Both Li and Ga show subtle differences in their corr(M,REE) versus ionic radius compared with the other LICE, such as clinopyroxene-favouring V and Sc (Fig. 9), which probably indicates that the bulk partitioning of Li and Ga have more of a contribution from olivine. Similarly, the appearance of both Fe and Cd in $\mathbf{V_5}$ (2+ elements) implies that the associations of variability exhibited by these two elements relates to the chemical properties of Fe and Cd during OFB petrogenesis.

A strong pattern emerges from the first two eigenvectors, brought out by looking at the trends established by the REE, which may be extrapolated in one direction from La to the VICE, and in the other from Lu to LICE (Fig. 10). Another feature is that the variabilities of the MREE to HREE (Gd to Lu) are partitioned differently between $\mathbf{V_1}$ (which affects Lu most) and $\mathbf{V_2}$ (which affects Gd most), despite these REE having almost identical total variabilities (Fig. 3). Many of the non-REE HICE follow the REE closely, suggesting that understanding the pattern of the distribution of the REE would appear to be an essential first step. Other elements plotting away from the trends defined by the REE in $\mathbf{V_1}$ and $\mathbf{V_2}$ are the plagioclase-affiliated elements Sr and Na ($\mathbf{V_1}$ and $\mathbf{V_3}$), and the potentially chalcophile elements Mo, Pb, Tl and to a lesser extent Sn.

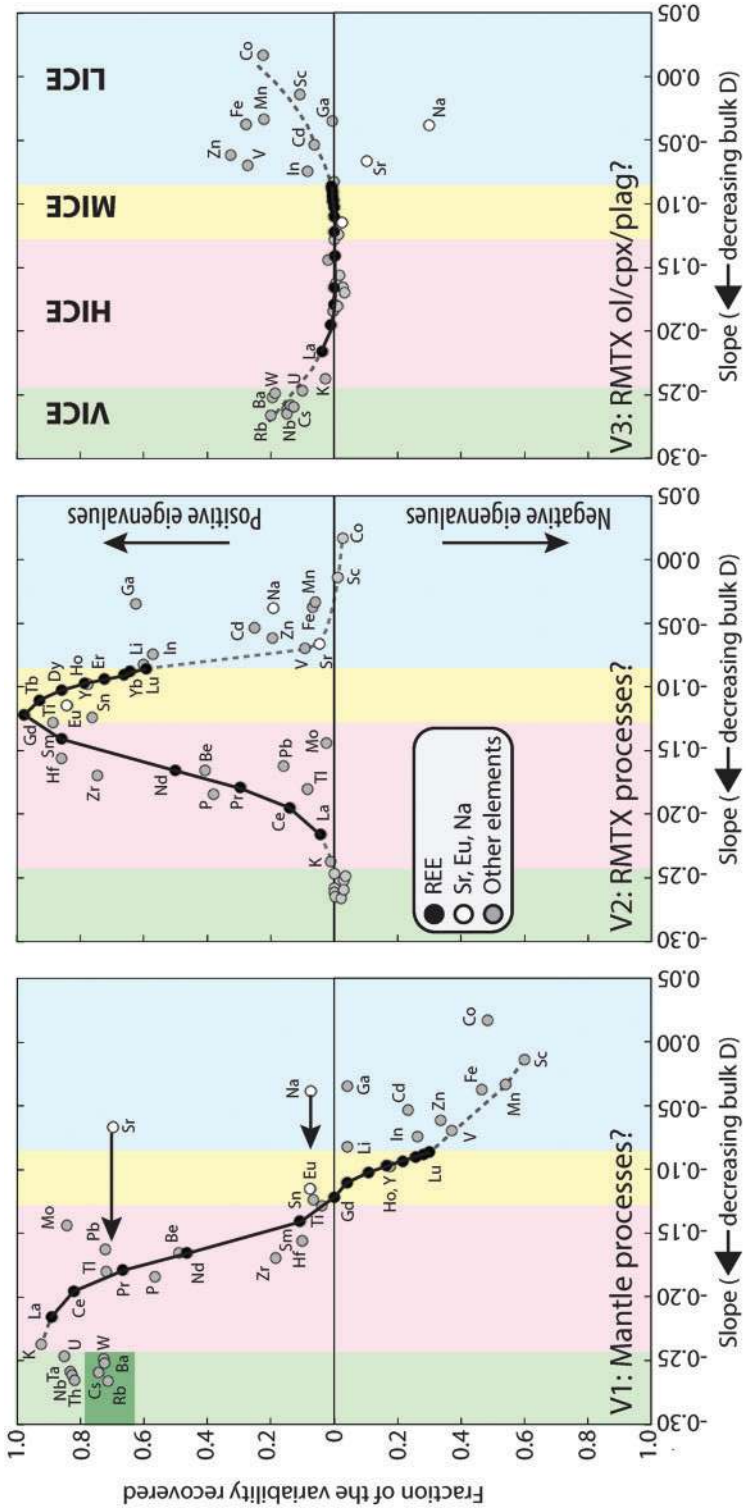

Fig. 10. Principal component analysis of the variabilities: the fraction of the variability recovered $[(a_{v_n,M})^2\lambda_n]$ for a given M by each of the first three eigenvectors versus slopes (values are given in Supplementary Data Table 3). Positive and negative entries of the eigenvectors are distinguished in the upper and lower panels, respectively. (See text for details.)

A useful clue in interpreting the processes or properties behind an eigenvector is when the entry for an element is zero. The entries for the VICE in eigenvector $\mathbf{V_2}$ are nearly zero, hence this 'association of variability' reflects processes to which the VICE are insensitive; yet $\mathbf{V_2}$ is centred around the MREE Gd and Tb, which, although these MICE may not be quite as incompatible as the VICE, are still sufficiently incompatible that they should be coupled to the VICE if their variabilities were caused by differences in the degree of partial melting, for example. Another clue is that the entry for Sc in $\mathbf{V_2}$ (i.e. $a_{V_2,Sc}$) is also near zero, which may be related to the fact that the bulk partition coefficient, D_{Sc}, in the RMTX process is close to unity (O'Neill & Jenner, 2012, fig. 5). Accordingly, Sc variability is insensitive to many of the deviations from the global average RMTX process, such as not reaching steady state, or difference in fractions tapped (ϕ_T) to crystallized (ϕ_X) in each cycle, though not to the proportions of olivine to clinopyroxene to plagioclase crystallizing (f_{ol}:f_{cpx}:f_{plag}), which affects bulk D_{Sc}. Meanwhile, the contribution from $\mathbf{V_2}$ for Na, $(a_{V_2,Na})^2\lambda_2$ plots near the trend of the REE as extrapolated towards Sc, and amongst the other LICE, suggesting that its 'slope', our proxy for bulk *D*, is appropriate. By contrast, $(a_{V_1,Na})^2\lambda_1$ appears in the equivalent diagram for $\mathbf{V_1}$ at a position that is clearly anomalous for its slope, hence bulk *D*. Putting these observations together suggests that the processes behind $\mathbf{V_2}$ are those of crustal evolution by RMTX, rather than partial melting or source composition variability. One striking implication of this hypothesis is for Sm–Nd isotope systematics. Fractionation of Nd from Sm is often assumed to be entirely due to partial melting (see Hofmann, 2003, and references therein), involving an effect of low-degree melts. Our analysis of variability demonstrates that RMTX processes also fractionate Nd from Sm significantly. Similarly, RMTX processes contribute to the scatter in $^{143}Nd/^{144}Nd$ versus La/Sm for global OFB (e.g. Hofmann, 2003, fig. 14). La/Sm does not solely reflect mantle source fertility or degree of partial melting during OFB petrogenesis.

Eigenvector $\mathbf{V_1}$ holds most of the variabilities of the VICE, and also a significant portion of the variabilities of some of the HICE (e.g. La), MICE (e.g. Lu) and LICE (e.g. Sc). However, the VICE and the HICE are anti-correlated with the MICE and the LICE. Both $a_{V_1,Sr}$ and $a_{V_1,Na}$ plot anomalously relative to the REE trend in $\mathbf{V_1}$, but the anomalies would be removed if $a_{V_1,Sr}$ and $a_{V_1,Na}$ were plotted at positions appropriate to their incompatibilities in higher-pressure processes where plagioclase is not an agent (see arrows in Fig. 10). Thus $\mathbf{V_1}$ has a connection to mantle processes (i.e. partial melting) where plagioclase is unimportant. $\mathbf{V_1}$ also pulls out the differences between the Ba-VICE and Th-VICE groups, and all the VICE are decoupled from the overall HICE–MICE–LICE trend. This decoupling probably reflects the contribution of recycled material (e.g. the subducting slab) to the variability in the OFB source mantle, as discussed above.

The third eigenvector $\mathbf{V_3}$ is also mainly concerned with the VICE and the LICE. The stand-out feature is the anomalous signs of $a_{V_3,Na}$ and $a_{V_3,Sr}$, pointing again to the influence of plagioclase. We suggest that the processes behind $\mathbf{V_3}$ are associated with changing proportions of olivine to clinopyroxene to plagioclase (f_{ol}:f_{cpx}:f_{plag}) during crustal evolution by RMTX. It should be noted that the Ba-VICE and the Th-VICE cannot be distinguished in $\mathbf{V_3}$ (i.e. Cs plots closer to Nb than Rb), which endorses our interpretation that the differences in variabilities of the Ba-VICE and the Th-VICE (Fig. 3) are inherited from the OFB-source mantle.

The PCA of variability leads again to the conclusion that the plagioclase-loving elements Na, Sr and to some extent Eu behave differently from other incompatible elements. This has some important implications because of the significance that Na variability has been given in interpreting OFB chemistry.

DISCUSSION

Variability of Na and the distribution of mantle potential temperature beneath mid-ocean ridges

Part of the variability of OFB compositions may be caused by differences in the net degree of partial melting of the mantle that produces their parental liquids (F_{OFB}), and part of these differences in F_{OFB} may be caused by differences in mantle potential temperature (T_p). Potential temperature is a parameter that characterizes an adiabatic temperature gradient in the mantle, calculated by extrapolating the adiabatic gradient to the Earth's surface (McKenzie & Bickle, 1988); such a gradient is the limit towards which the transport of heat by convection trends. The concept really only has useful meaning for mantle where convection has been efficient enough that the temperature distribution with depth has approached an adiabatic gradient. Insofar as the upwelling of the mantle leading to OFB petrogenesis is a passive process, OFBs may sample T_p without bias. Therefore, variations in OFB chemistry may provide insight into the scale and efficiency of mantle convection.

Establishing the relationship between OFB chemistry and T_p requires three steps. The first is to relate the observed OFB compositions to parental melt compositions. Then the parental compositions need to be related to F_{OFB}, which requires information about the physical aspects of melt extraction as well as the source compositions. Finally, F_{OFB} is related to T_p, which is not straightforward because of dynamic factors including melt focusing and conductive cooling to the surface. The extreme case of the latter occurs at amagmatic ridge segments where F_{OFB} is zero (e.g. Dick *et al.*, 2003). However, if it could be assumed that the mantle source composition was constant, there might be a typical sensitivity, dF_{OFB}/dT_p, but only where the mantle upwelling approaches adiabaticity. More formally, although F_{OFB} is a function of source composition and

non-adiabaticity as well as T_p, if we take a specified constant source composition and negligible non-adiabaticity, and put $F_{OFB} = f(T_p)$, then a first-term Taylor's series expansion around the average mantle T_p ($\overline{T}_p$) gives $F_{OFB} = \overline{F}_{OFB} + dF_{OFB}/dT_p\ (T_p - \overline{T}_p)$, where $\overline{F}_{OFB}$ is the global average degree of melting, corresponding to $\overline{T}_p$.

Source composition affects matters in two ways: first, in mapping parental melt compositions onto values of F_{OFB}, and second, both F_{OFB} and the dF_{OFB}/dT_p sensitivities must to some extent depend on source composition, especially on contributions from non-peridotitic lithologies (e.g. Cordery *et al.*, 1997) and H_2O contents (e.g. Asimow *et al.*, 2004). It should be mentioned here that not all geochemists are convinced that OFB or indeed many other basalts result from melting monolithological peridotite sources (e.g. Lambart *et al.*, 2013, and references therein). For example, Sobolev *et al.* (2007) proposed that mid-ocean ridge basalts contain 10–30% pyroxenite-derived melt. Evaluating dF_{OFB}/dT_p sensitivities is beyond the scope of this study, but some estimates from the literature can be noted.

Another way of estimating F_{OFB} and hence T_p is from crustal thickness (e.g. McKenzie & Bickle, 1988). As this approach is less sensitive to the reconstruction of parental melt compositions from observed OFB compositions, it provides a test of the basalt chemistry calculations. The basalt chemistry approach was promulgated in a seminal paper by Klein & Langmuir (1987), who showed that variations in basalt chemistry from mid-ocean ridges correlated with depth beneath sea level to the ridge axis, which they proposed was due to variable T_p. They drew particular attention to the variability of Na and Fe, but other elements and element ratios (such as Ca/Al) were also considered. They found that Na and Fe were positively correlated during the low-pressure evolution of MORB, which is expected as both elements behave moderately incompatibly during crystallization of basaltic magmas. But when local trends of Na and Fe vs MgO were projected to 8 wt % MgO, the resulting projected values, called Na_8 and Fe_8, were somewhat anticorrelated. Broadly speaking, similar behaviour is found in the global OFB dataset of Jenner & O'Neill (2012*a*): the slopes d(log[Na])/d[MgO] and d(log[Fe])/d[MgO] are identical (Fig. 3), whereas the variabilities of Na and Fe are anticorrelated (Figs 8–10).

Klein & Langmuir (1987) ascribed the variations of Na_8 to differences in F_{OFB}. As expected of any element that behaves incompatibly during melting, the lower the F_{OFB}, the higher the element's concentration in the derived melt, assuming constant source composition. In the case of magmatism at mid-ocean ridges, the cooler the mantle, the shallower the depth at which the T_p trajectory of the upwelling mantle intersects the *T–P* curve of the peridotite solidus, and the less melt is produced. Meanwhile, according to Klein & Langmuir (1987), Fe_8 is an indicator of the average pressure of melting. Low-degree melts (with higher Na) should originate in a melting column initiating at lower pressure, hence the anti-correlation of Fe_8 with Na_8. Klein & Langmuir (1987, fig. 12) gave quantitative relationships between T_p, F_{OFB} and crustal thickness. The sensitivity dF_{OFB}/dT_p was $\sim 4 \times 10^{-4\circ}C^{-1}$.

The original work of Klein & Langmuir (1987) has been updated through expanded expositions of their arguments (Klein & Langmuir, 1989; Langmuir *et al.*, 1992), followed more recently by the publication of a greatly augmented database of MORB compositions allowing Na_8 to be calculated for 241 segments of the global ridge system (Gale *et al.*, 2013, 2014). Nevertheless, all this additional work has not changed the original conclusions of Klein & Langmuir (1987) regarding variations in T_p. Klein & Langmuir (1987) stated that: 'Beneath the shallowest and deepest ridge axes, temperature differences of approximately 250°C in the subsolidus mantle are required to account for the global systematics'. This temperature variation was inferred to correspond to regional variations in $\overline{F}_{OFB}$ from 8 to 20% (implying dF_{OFB}/dT_p of $4{\cdot}8 \times 10^{-4\circ}C^{-1}$), and to produce primary magmas with [MgO] from 10 to 15 wt % MgO. Referring to their expanded database of 241 ridge segments, Gale *et al.* (2014) stated that: 'A mantle temperature range of ~200°C best explains the correlations', where the correlations referred to are of major elements and ridge depth. Dalton *et al.* (2014) investigated the relationship between mantle temperature structure derived from the Klein & Langmuir approach with regional shear-wave velocities, and opted for '250°C variation extending to depths >400 kilometres'.

Mapping variations in Na_8 onto T_p has not gone unchallenged (e.g. Niu & O'Hara, 2008), as Gale *et al.* (2014) have acknowledged. Others have used petrological arguments to arrive at seemingly different conclusions, as pointed out by Herzberg *et al.* (2007) and Putirka *et al.* (2007), for example. Both Herzberg *et al.* (2007) and Purtirka *et al.* (2007) used olivine–melt equilibria to infer T_p, albeit with different strategies and parameterizations, with compositions of the parental liquids estimated from the observed OFB compositions, assuming crustal evolution by simple fractional crystallization (SFX). Herzberg *et al.* (2007) quoted their result as a range of T_p of 120°C (1280–1400°C), whereas Purtirka *et al.* (2007) found a higher average temperature (1466°C) with a similar range (140°C), for which they also gave a standard deviation, $\sigma(T_p)$ of ±34°C; both of these are significantly lower than the 250°C variations predicted using the Klein & Langmuir approach.

Estimates of T_p variability from seismically determined crustal thicknesses are considerably lower. Here we add the caveat that a definition of 'crust' based on physical properties may not correspond exactly to a petrological definition (e.g. Cannat, 1996). Petrological definitions vary, but for this discussion we adopt the one that uses the petrogenetic origins of the lithologies: the mantle is the residual peridotite that remains after varying degrees of melt extraction, whereas the crust is composed of the crystallization products from the

extracted melts (Pirard *et al.*, 2013). With this definition, the petrological crustal thickness Z_{pet} should reflect F_{OFB}, such that the standard deviation in global average degree of melting, $\sigma(\overline{F}_{OFB})$ and hence $\sigma(T_p)$ should be proportional to that in the petrological crustal thickness, $\sigma(Z_{pet})$. Let the difference between the geophysically determined crustal thickness, Z_g, and Z_{pet} be Δz, such that $Z_{pet} = Z_g + \Delta z$. The difference Δz could be positive (e.g. ultramafic cumulate such as dunite assigned to Z_g), or negative (e.g. serpentinized mantle peridotite included in Z_g). By propagation of error, $\sigma(Z_{pet})^2 = \sigma(Z_g)^2 + \sigma(\Delta z)^2 + 2\sigma(Z_g)\sigma(\Delta z)\mathrm{corr}(Z_g,\Delta z)$, where $\mathrm{corr}(Z_g,\Delta z)$ is the correlation coefficient between Z_g and Δz. Unless this correlation coefficient is negative, $\sigma(Z_{pet})$ cannot be less than $\sigma(Z_g)$. A negative correlation coefficient would mean that the larger the value of Z_g, the smaller Δz. Although conceptually this might happen where Z_{pet} is small or zero, with mantle peridotite exposed, it seems a trivial possibility given that values of Z_g are not likely to be reported from such areas, which would anyway be excluded if ultraslow-spreading ridges are excluded (see below). Elsewhere, negative $\mathrm{corr}(Z_g,\Delta z)$ seems unlikely; rather, it is surely to be expected that the thicker the crust, the larger Δz and $\sigma(\Delta z)$; for example, owing to an increase in cumulate dunite. Hence, inferring $\sigma(\overline{F}_{OFB})$ from global estimates of $\sigma(Z_g)$ should if anything exaggerate $\sigma(\overline{F}_{OFB})$, and hence $\sigma(T_p)$.

Bown & White (1994), followed by White *et al.* (2001), proposed that the relatively constant thickness of the ocean crust ($Z_g = 6{\cdot}3 \pm 0{\cdot}9$ km) corresponds to a variation in T_p of $\pm 20^\circ$C, based on the parameterization of mantle melting of McKenzie & Bickle (1988). The relationship between crustal thickness and T_p given by Klein & Langmuir (1987) (e.g. in their fig. 12) suggests about half this. Katz (2010) pointed out that the way melt is focused from the melting zone may influence the relationship between crustal thickness and T_p, leading Gregg *et al.* (2012) to suggest that the $\pm 0{\cdot}9$ km variation in thickness corresponds to $\sigma(T_p)$ of $2{\cdot}5^\circ$C only.

Crustal thickness is independent of spreading rate down to spreading rates of $\sim 1{\cdot}5$ cm a^{-1} (Bown & White, 1994), below which the thickness is highly variable, but typically lower, as found at the South West Indian Ridge and Gakkel Ridge, where it goes to zero thickness along some sections, exposing mantle peridotite (Dick *et al.*, 2003). The lower thickness at the ultraslow-spreading ridges implies lower melt productivity, which is consistent with some conductive heat loss during upwelling, which depresses the depth at which melting ceases (Bown & White, 1994). Elsewhere, it is assumed that the melting process is essentially adiabatic, under which circumstances F_{OFB} and hence crustal thickness would reflect mantle potential temperature (T_p), if the mantle source composition were constant, and if the geometry of the two-phase flows (melt and residue) were also constant. According to Bown & White (1994) and White *et al.* (2001), the spread of normal crustal thickness of $\pm 0{\cdot}9$ km corresponds to a spread in T_p of $\pm 20^\circ$C for a constant source composition, although Gregg *et al.* (2012) stated that the temperature distribution may be only $\pm 2{\cdot}5^\circ$C as a result of melt focusing, based on the work of Katz (2010). Su & Buck (1993) modelled crustal thickness and spreading rate as a function of T_p; their model finds that the sensitivity of crustal thickness to T_p depends on spreading rate, becoming more sensitive below about 1·5 cm a^{-1}, in agreement with the observations. At 3 cm a^{-1}, their model gives a sensitivity of thickness to T_p of 0·14 km $^\circ$C^{-1}, so that $\pm 0{\cdot}9$ km implies $\sigma(T_p)$ of $\pm 6{\cdot}4^\circ$C.

Part of the apparent disagreement can be traced to semantics. There are two issues: what parts of the mantle are being referred to when T_p variations are quoted, and what a 'range of temperature' signifies. With regard to the first issue, we note that the temperature structure of the mantle on a global scale is expected to reflect its two modes of global-scale convection, the plate mode and the plume mode. In the aphorism of Davies (e.g. Davies, 2011, p. 105): 'Plates cool the mantle, whereas plumes cool the core'. Both modes produce basalt: plate tectonics produces OFB by more-or-less passive upwelling of mantle into the region where the plates are rifting apart, whereas plumes produce basalt by active upwelling induced by thermal buoyancy, meaning higher T_p. The two modes interact to some extent, if only by coincidence. At Iceland, a major plume coincides with the rifting plates, causing a dramatic increase in crustal thickness, from the canonical $6{\cdot}3 \pm 0{\cdot}9$ km of the typical oceanic crust up to a maximum thickness of 46 km, with an average of 29 km (Allen *et al.*, 2002). Less extreme but still noticeably thicker crust (*c.* 15 km) is found near the Azores plume (Louden *et al.*, 2004), whereas the crust produced at the Galapagos Ridge thickens by only ~ 2 km with proximity to the Galapagos plume (Canales *et al.*, 2002).

The increase in crustal thickness at Iceland has been ascribed to a temperature excess of 100–200°C in the Iceland plume. Iceland has often not been considered the strongest plume: for example, according to the recent appraisal of King and Adam (2014), that honour would go to Hawaii, with a buoyancy flux three times larger than Iceland's. However, Jones *et al.* (2014) and Parnell-Turner *et al.* (2014) disagreed, putting the Icelandic plume flux at up to five times that of the Hawaiian plume. This is a significant point, because if these latter researchers are correct, it would greatly reinforce the idea that Iceland is a unique phenomenon in the distribution of T_p in sub-ridge mantle.

If the extra 22 km or so of crustal thickness at Iceland is due to an excess temperature of 200°C, then proportional scaling would suggest that the $\pm 0{\cdot}9$ km variation in the thickness of normal oceanic crust corresponds to $\pm 8^\circ$C. This is the kind of sensitivity of melt productivity to mantle T_p found by both Klein & Langmuir (1987; see their fig. 12) and McKenzie & Bickle (1988; see their figs 7b and 15d), although it is still rather larger than the estimate of Gregg *et al.* (2012) of $\pm 2{\cdot}5^\circ$C. Although Iceland is a unique phenomenon on the present-day

global ridge system, two other plumes on ridges have produced anomalously thick oceanic crust in the last 100 Myr. The Tristan plume produced the greatly thickened crust of the Walvis Ridge–Rio Grande Rise when it was below the Mid-Atlantic Ridge between 60 and 128 Ma, and the Reunion plume produced a ridge on both sides of the spreading centre on the Carlsberg Ridge between 40 and 60 Ma (Campbell, 2007). The V-shaped ridges to the north and south of Iceland (Vogt, 1971) have been ascribed to thermal pulses in the Iceland plume (Poore *et al.*, 2009; Jones *et al.*, 2014; Parnell-Turner *et al.*, 2014). These observations provide compelling evidence that crustal thickness is very sensitive to T_p.

As both Herzberg *et al.* (2007) and Putirka *et al.* (2007) have emphasized, the parts of the ridge system used by Klein & Langmuir (1987), Dalton *et al.* (2014) and Gale *et al.* (2014) to state that mantle T_p ranges over 200 or 250°C include Iceland. It is questionable whether it is useful to include this currently unique on-ridge plume locality into estimates of mantle T_p variability, while excluding other parts of the mantle away from ridges that sample the plume mode, such as Hawaii. Indeed, Putirka *et al.* (2007) pointed out that a misinterpretation of this issue misled Anderson (2000) into supposing that: 'If normal mantle temperatures are 1400°C ± 200°C... there is no thermal requirement for hot mantle plumes'. Putirka *et al.* (2007) went on to say that 'their 250°C range clearly represents $T_{Iceland}$ – $T_{coldest\ MORB}$', but this may also be misleading, because the 'coldest MORB' referred to here are from ultraslow-spreading ridges, which raises a different issue. While the thin crust at many such ridge segments points to low F_{OFB} (and no crust means zero F_{OFB}), this is not necessarily because of lower T_p; rather, it is likely that conductive cooling causes the melting of the upwelling mantle to cease at a greater depth (Bown & White, 1994; White *et al.*, 2001) or not to melt at all (Dick *et al.*, 2003). Hence basalts from ultraslow-spreading ridge segments should not be included in estimating the distribution of T_p without making a correction for non-adiabaticity, which adds an extra layer of difficulty. Here we define such segments as those with spreading rates <15 mm a^{-1}, based on White *et al.* (2001). In the extreme cases of the amagmatic parts of ultraslow-spreading ridges, where no basaltic crust is produced (e.g. Dick *et al.*, 2003), the absence of basalt would, logically, lead to a sampling bias on T_p if this effect were ignored. One point of interest is that in the original work of Klein & Langmuir (1987), the anti-correlation between high Na_8 and low Fe_8 was leveraged at the high Na_8 end of their array by data from the Cayman Spreading Centre. These segments have the greatest depth to the ridge of any (>5000 m). Although they were categorized as ultraslow spreading by White *et al.* (2001), with a spreading rate of 11 mm a^{-1}, Gale *et al.* (2014) listed them at 19 mm a^{-1} (see also DeMets & Wiggins-Grandison, 2007). The crust at the Cayman Spreading Centre is very thin [1·9–4·6 km according to White *et al.* (2001)], which Stroup & Fox (1981) suggested was due to adjacent transform faults acting as a heat sink. Whatever the explanation, it would be over-optimistic to suppose that the basalt chemistry and melt productivity at the Cayman Spreading Centre could be mapped onto T_p in the same way as for basalts at normal ridge segments, and we shall follow White *et al.* (2001) rather than Gale *et al.* (2014) in classifying these segments as ultraslow spreading.

The other semantic issue is what is meant by a range of T_p. Ranges, defined as the difference between the highest and the lowest values sampled from a population, do not provide particularly informative descriptions of distributions (i.e. probability density functions), one reason being that they depend on the number of samples taken from the population. If the distribution of T_p in the sub-ridge mantle were Gaussian, then for 241 samples [the number of ridge segments considered by Gale *et al.* (2014)], the most probable value of the standard deviation would be given by the range divided by 5·5 (Tippett, 1925). So the range of 200°C quoted by Gale *et al.* (2014) would probably correspond to a standard deviation of about 35°C. However, the distribution of melt productivity to be mapped onto T_p beneath the ridge system is not likely to be Gaussian. Rather, as seen from the above discussion, the net distribution that we might expect is a convolution of four sub-distributions, such that we might expect the following: (1) a main peak in the distribution corresponding to the canonical 6·3 ± 0·9 km crustal thickness; (2) a shoulder at lower F_{OFB} from the ultraslow-spreading segments; (3) a shoulder at higher F_{OFB} corresponding to the presence of nearby but off-axis plumes, such as the Azores; (4) a well-resolved peak for Iceland. We suggest that a clearer picture of mantle T_p associated with the plate mode would be obtained if both the ultraslow-spreading segments and Iceland were removed from consideration. In view of the criticism regarding geochemists postulating 'plumes' to filter geochemical data along the global ridge system (e.g. Anderson, 2000), we feel that it is safer not to exclude anything else apart from Iceland and its adjacent spreading regions on the grounds of supposed plume influence. Plume-influenced mantle may have a systematically different composition, including having a higher H_2O. For example, Asimow *et al.* (2004) have argued that the greater thickness of the crust at the Azores may be partly due to higher H_2O enhancing melt productivity, not just higher T_p. The downside of not filtering out non-Icelandic plumes is that the apparent distribution of mantle T_p derived from basalt chemistry may be biased in two ways: a real increase in the frequency of T_p values at the high-T_p end of the distribution, because plume-affected mantle is indeed hotter; and a false contribution from the assumption of constant source composition because plume-affected mantle will have a higher dF_{OFB}/dT_p and $\overline{F}_{OFB}$ (e.g. Asimow *et al.*, 2004).

Gale *et al.* (2014) reported major element data for 241 ridge segments or combinations of segments

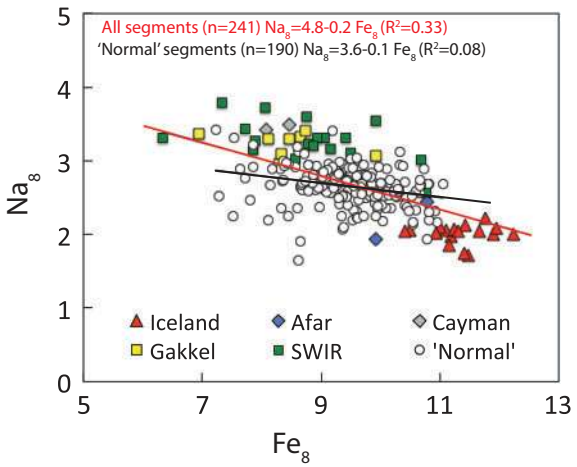

Fig. 11. Variations in Fe_8 versus Na_8 for 241 segments of the global ridge system (Gale *et al.*, 2013, 2014). From these segments we have filtered out the ultraslow-spreading segments, Iceland and samples collected just south of Iceland located from 57°N to 69°N, which leaves 190 segments. Removing these anomalous ridge sections shows that the anti-correlation between Fe_8 versus Na_8 is lost (R^2 drops from 0·33 to 0·08). SWIR, South West Indian Ridge.

averaged and projected onto 8 wt % MgO. We remove from consideration the ultraslow-spreading segments (Gakkel, nine segments; South West Indian, 21 segments; Afar, two segments; Cayman, two segments), and Iceland plus the anomalous part of the Mid-Atlantic Ridge to the south, with its V-shaped ridges (Vogt, 1971; Poore *et al.*, 2009; Jones *et al.*, 2014; Parnell-Turner *et al.*, 2014); that is, from 57°N to 69°N, comprising 17 segments. This leaves 190 segments. The correlation between Na_8 and Fe_8 claimed by Klein & Langmuir (1987) is lost, as shown in Fig. 11, with R^2 of only 0·08 (a drop from an already poor R^2 of 0·33 when including all 241 segments). The mean Na_8 is 2·65 wt %, with a standard deviation $\sigma(Na_8)$ of 0·27 wt % (i.e. 10%).

If the variation of Na_8 shown in Fig. 11 was due entirely to differences in degree of partial melting of a compositionally uniform source, it could be mapped onto $\overline{F}_{OFB}$ fairly easily, as may be shown, for example, by applying the model of Niu & Batiza (1991), which is attractive for its simplicity, hence transparency. Niu & Batiza (1991) calculated the compositions of parental OFB melts from an accumulated, near-fractional, polybaric melting model parameterized from experimentally determined phase equilibria, which predicted parental melts with 10–12 wt % MgO. They then assumed that these melts evolved by closed-system simple fractional crystallization (SFX) to 8 wt % MgO, from which they obtained $F_{OFB} = 0{\cdot}192 - 0{\cdot}052\ Na_8 + 0{\cdot}155\ Ca_8/Al_8$ [equation (9) of Niu & Batiza (1991)]. Using the values of Na_8, Ca_8 and Al_8 given by Gale *et al.* (2014) for the 190 selected ridge segments gives $\overline{F}_{OFB} = 0{\cdot}176 \pm 0{\cdot}020$. This global average $\overline{F}_{OFB}$ depends on the Na content of the experimental composition used in the parameterization matching that in the source composition, which is questionable (as is the assumption of constant source composition), but the standard deviation $\sigma(F_{OFB})$ of $\pm 0{\cdot}020$ should hardly be affected by this problem. With a sensitivity of $5 \times 10^{-4\circ}C^{-1}$, this implies $\sigma(T_p) = 40°C$, similar to the estimate of Putirka *et al.* (2007). Using the relationship between F_{OFB} and the initial pressure of melting, P_o, given by Niu & Batiza (1991), their equation (8) (P_o/kbar $= 25{\cdot}98 + 0{\cdot}967\ F_{OFB} + 45{\cdot}277/F_{OFB} - 5{\cdot}186\ Si_8/Fe_8$), with the parameterization of the mantle peridotite solidus of Hirschmann (2000) (T/°C $= 1121 + 133\ P - 0{\cdot}051\ P^2$), also gives the same result, $\sigma(T_p) = 40°C$, with $\overline{T}_p = 1340°C$.

Thus there remains a discrepancy in estimates of the distribution of mantle T_p beneath ridges (excluding Iceland) between those from basalt chemistry, with $\sigma(T_p) \sim 40°C$, and those from crustal thicknesses, with $\sigma(T_p)$ mostly $< 10°C$. The analysis of OFB compositional variability in our study suggests that this is probably due to two invalid assumptions in the basalt chemistry approach: assuming simple fractional crystallization (SFX) rather than RMTX to calculate parental magma compositions, either from observed OFB compositions directly, or from compositions projected to 8 wt % MgO, and the assumption of constant source composition.

RMTX versus SFX in producing variability of Na_8 and Fe_8

Simple fractional crystallization (SFX) should cause little variability in Na_8 for a given parental melt composition, the main effect being the change of f_{ol}:f_{cpx}:f_{plag} with pressure, which is not great within the crustal pressure range of ~0·5 to 3 kbar at which much of the SFX is likely to occur. Under such a paradigm there is no option but to deduce that most of the observed compositional variability in Na_8 is inherited from that in the parental magmas. But as O'Hara (1977) pointed out, RMTX processes allow the possibility of greater degrees of compositional variability being introduced during low-pressure evolution, so less variability should be ascribed to the parental magmas. In an idealized steady-state RMTX magma chamber, variability in Na_8 may conceptually result from two end-member possibilities: (1) varying ϕ_X/ϕ_T at constant f_{ol}:f_{cpx}:f_{plag}; (2) varying f_{ol}:f_{cpx}:f_{plag} at constant ϕ_X and ϕ_T. The consequences of the first possibility are shown in Fig. 12. Compared with SFX, steady-state RMTX always produces higher [Na] for a given parental magma composition ($[Na]_o$). The effect of RMTX might be cryptic, as in the hypothetical case that a parental magma with >10 wt % MgO evolves to an intermediate [MgO] by RMTX (say, 8 wt %), from which point on the magma chamber is tapped periodically without replenishment to produce a suite of cogenetic magmas (with [MgO] from 8 wt % downwards) related by SFX. This possibility is illustrated in Fig. 12, labelled 'hybrid'. We also show that the assumption that Na_8 from an observed suite of OFB magmas is related to the $[Na]_o$ in the parental magma only by SFX (i.e. the projection of the

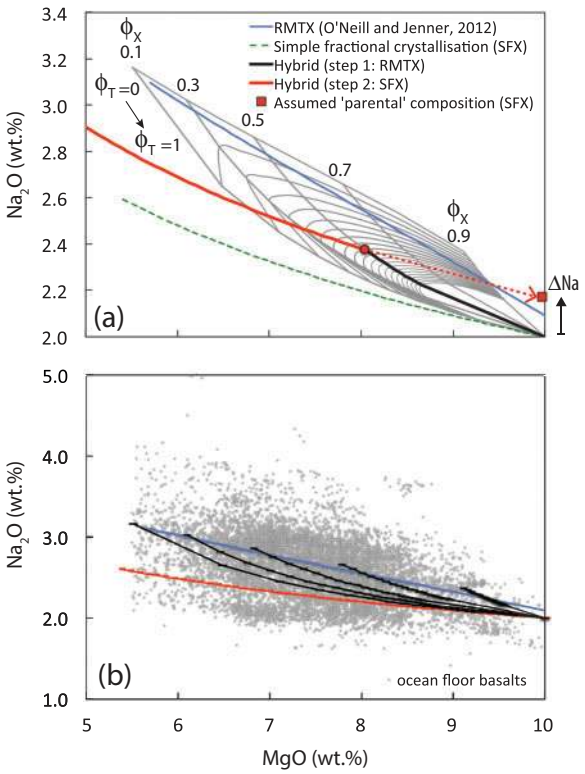

Fig. 12. (a) Na_2O versus MgO variations for RMTX with varying ϕ_X/ϕ_T at constant f_{ol}:f_{cpx}:f_{plag} compared with modelling of SFX and a hydrid RMTX + SFX model (see text for further details). Assuming Na_8 is related to the parental magma by SFX results in an overestimate of the Na content of the parental melt. (b) Comparison of RMTX and SFX modelling lines with variations in Na_2O versus MgO for the Smithsonian Abyssal Volcanic Glass Database (Melson *et al.*, 2002).

model line to [MgO] 10 wt %) will give an erroneously high estimate of the [Na] of the parental melt (offset shown as ΔNa in Fig. 12).

The effects of changing the fractions of f_{ol}:f_{cpx}:f_{plag} on Fe_8 and Na_8 may be investigated by forward modelling. Starting from the model of O'Neill & Jenner (2012), we apply the constraint that values of ϕ_X and ϕ_T should only vary along a path reproducing the minimum limiting slope d(log[M_{VICE}])/d[MgO] for a perfectly incompatible element (bulk $D_{VICE} = 0$) of –0·26, as found in the global array. We take parental $[Mg]_o = 10{\cdot}4$ wt % (O'Neill & Jenner 2012). Values of D_{MgO} were then varied between 1·5 and 2·6, with the constraints that $f_{ol} + f_{cpx} + f_{plag} = 1$, and $D_{MgO} = D_{MgO}^{plag/melt} f_{plag} + D_{MgO}^{cpx/melt} f_{cpx} + D_{MgO}^{ol/melt} f_{ol}$. Using the partition coefficients for Fe and Na from O'Neill & Jenner (2012), values of Fe_8 and Na_8 were calculated relative to parental magma values $[Fe]_o$ and $[Na]_o$, and the results were parameterized, approximately, by fitting to linear relations:

$$\log(Fe_8/[Fe]_o) = 0 \cdot 38 - 0 \cdot 29 f_{cpx} - 0 \cdot 77 f_{ol} \quad (11a)$$

$$\log(Na_8/[Na]_o) = -0 \cdot 17 + 0 \cdot 43 f_{cpx} + 0 \cdot 53 f_{ol}. \quad (11b)$$

From Fig. 11, the array for 'normal' ridge segments runs from about $Na_8 = 3{\cdot}5$ wt %, $Fe_8 = 7$ wt % to $Na_8 = 2{\cdot}0$ wt %, $Fe_8 = 11$ wt %. If we assume $[Na]_o = 2{\cdot}0$ wt % and $[Fe]_o = 8{\cdot}0$ wt %, these limits correspond to $f_{ol} = 0{\cdot}39$, $f_{cpx} = 0{\cdot}48$ and $f_{plag} = 0{\cdot}13$, and $f_{ol} = 0{\cdot}31$, $f_{cpx} = 0{\cdot}68$ and $f_{plag} = 0{\cdot}02$. A typical OFB with $Na_8 = 2{\cdot}65$ wt % at $Fe_8 = 9{\cdot}5$ wt % implies $f_{ol} = 0{\cdot}26$, $f_{cpx} = 0{\cdot}36$ and $f_{plag} = 0{\cdot}38$. This calculation is presented only as an example to demonstrate that the entire field of Na_8 and Fe_8 could in principle be reproduced just by varying f_{ol}:f_{cpx}:f_{plag}. Removing the constraint in the forward modelling on ϕ_X and ϕ_T, which is made only for illustrative purposes, would increase the range of $\log(Na_8/[Na]_o)$ and $\log(Fe_8/[Fe]_o)$ accessed by changing f_{ol}:f_{cpx}:f_{plag} even further.

This raises the question of how much variability in f_{ol}:f_{cpx}:f_{plag} is reasonable. Experimental petrology shows that plausible OFB parental magmas evolve through the crystallization sequence ol → ol + plag → ol + plag + cpx at low pressures, but that the position of the cotectics changes with pressure (e.g. Presnall *et al.*, 1978; Whitaker *et al.*, 2007). Compositional effects such as increasing H_2O content or decreasing Al_2O_3, either from higher pressure of melting or lower degree of melting, also expand the phase volume of cpx relative to plag, ultimately leading to the sequence ol → ol + cpx → ol + plag + cpx, as is typical of ocean island or island arc basalts (Perfit *et al.*, 1980; Albarède, 1992). In RMTX processes, the effects of small changes in the locus of the ol + plag + cpx cotectic are magnified over many cycles to have large effects on the net f_{ol}:f_{cpx}:f_{plag} crystallized. Another related effect may be understood from the fact that whereas the phase relations in tholeiitic OFB basalts at [MgO] > 5·5 wt % involve only three crystallizing phases (ol, plag and cpx), a four-component system has long been considered necessary for their description, namely the traditional basalt tetrahedron, Olivine–Plagioclase–Clinopyroxene–SiO_2 (Yoder & Tilley, 1962; O'Hara, 1965). Repeated cycles of crystallization of ol, plag and cpx cause the build-up of the fourth component SiO_2, leading eventually to saturation in low-Ca pyroxene, which has been found as a cumulate phase in lower crustal 'gabbros' (Gillis *et al.*, 2014). Crystallizing significant amounts of low-Ca pyroxene would not be expected if the dominant process were SFX. Hence, for a given parental magma, the steady-state SiO_2 content depends on the balance between ϕ_X and ϕ_T that also controls trace element abundances (i.e. flux in versus flux out). The cotectic phase relations in the system CaO–MgO–Al_2O_3–SiO_2 (CMAS) determined by Libourel *et al.* (1989) show that the build-up of SiO_2 expands the phase volumes of ol and plag at the expense of cpx when projected from SiO_2 onto Forsterite–Anorthite–Diopside. This is one example of how the physical characteristics of the volcanic plumbing system may influence the locus of the cotectic, in addition to the depth of the magma chamber.

Another remarkable influence on the position of the ol + plag + cpx cotectic was documented by Biggar & Humphries (1981), who studied the addition of Na_2O to CMAS. They found that increasing Na/Ca expands the phase volume of cpx at the expense of plag (see Biggar

& Humphries 1981, fig. 4). This effect has the potential of setting up a positive-feedback loop in an RMTX magma chamber, in which crystallization of a high ratio f_{cpx}/f_{plag} increases Na/Ca, thereby leading to even higher f_{cpx}/f_{plag} (and vice versa).

Estimating the contribution of RMTX processes to the variability of Na_8

The above discussion establishes the possibility that some part of the variability of Na_8 may be due to RMTX processes that are not accounted for by assuming that Na_8 is derived from $[Na]_o$, the concentration in the parental magmas, by SFX. Modelling the evolution of Macquarie Island basalts (Kamenetsky & Eggins, 2012) by O'Neill & Jenner (2012) indicates also that a considerable difference in f_{ol}:f_{cpx}:f_{plag} from the global trend may be possible (0·06:0·85:0·09 for Macquarie Island vs 0·18:0·42:0·41 for the global trend).

We have presented three observations that confirm that variability in parental $[Na]_o$ cannot be retrieved from that observed in Na_8 by correcting only for SFX, as follows.

1. Part of the variability of Na is correlated with that of Sr and the Eu anomaly (Figs 9 and 10).
2. The variability of Na is partly anticorrelated with those of other MICE or LICE, whose abundances in parental OFB should reflect the extent of partial melting (Fig. 10).
3. Variability in Na increases with low-pressure evolution (Fig. 7).

The first two observations point to the influence of variable f_{ol}:f_{cpx}:f_{plag} whereas the third is less specific, covering other factors such as the variability of ϕ_T and ϕ_X in steady-state RMTX magma chambers (Fig. 12), or not reaching steady state (Coogan & O'Hara, 2015). Taken together, these observations suggest that up to half the variability of Na_8 ascribed previously to difference in T_p may be due instead to RMTX processes.

The effect of source composition on Na_8

As has been emphasized repeatedly in this discussion, the mapping of F_{OFB} onto T_p is done under the enabling assumption that the Na content of the source is uniform. Clearly though, the abundances of the VICE and HICE in the OFB-source mantle are heterogeneous, as is also shown by the distributions of radiogenic isotopes (e.g. Hofmann, 2003; Stracke, 2012). Given this heterogeneity, it seems implausible that the same mantle is completely homogeneous in MICE and LICE (see Fig. 3). To constrain the Bulk Silicate Earth abundance of Na, O'Neill & Palme (1998) examined [Na] in 20 suites of upper mantle peridotites, extrapolating trends of [Na] vs [MgO] to their presumed Bulk Silicate Earth value of 36·8 wt % MgO. Projecting onto a constant [MgO] makes allowance for previous episodes of depletion or refertilization. The concentration of [Na] at 36·8 wt % MgO is 2380 ppm with a standard deviation of 360 ppm (i.e. 15%), actually a little larger than for other LICE (V, Cr, Mn, Co, Zn and Ga), for which the standard deviation is 6–12%. A 15% standard deviation is more than enough to account for the observed dispersion of Na_8 in the population of 'normal' ridge segments listed by Gale *et al.* (2014) and plotted in Fig. 10, for which the standard deviation is 10%. There is no empirical evidence from actual upper mantle peridotites to support the hoped for assumption that they are compositionally homogeneous in Na at the $< 10\%$ level, as demanded by the hypothesis that source heterogeneity can be neglected.

In a parallel universe, there exists a different paradigm of basalt source composition. For example, Sobolev *et al.* (2007) have suggested that pyroxenite-derived melts contribute 10–30% to mid-ocean ridge basalts. Sobolev *et al.* (2007) did not address the implications of their model for any part of the model of Langmuir and co-workers (Klein & Langmuir, 1987; Langmuir *et al.*, 1992), let alone for specific details such as the variability of Na_8. Conversely, neither Gale *et al.* (2014) nor Dalton *et al.* (2014) addressed the implications of any pyroxenite in the source.

Correlation between Na_8 and depth to the ridge axis

The correlation between Na_8 and depth to the ridge axis discovered by Klein & Langmuir (1987) remains after removing Iceland and the ultraslow-spreading ridges (Fig. 13a). Following their claim that the variability of Na_8 was due to differences in F_{OFB}, hence T_p, it was logical for Klein & Langmuir (1987) to ascribe the variation in ridge depth also to T_p. However, although the topography of mid-ocean ridges may well depend on their local underlying temperature structures, it is not clear that these temperature structures depend much on T_p, a property that has meaning only in relation to the convecting mantle beneath where melt extraction starts. As the conventional explanation for ridge elevation above the abyssal sea floor is that it is dynamic topography caused by mantle upwelling, it seems likely that differences in axial depth might be due to differences in the details of this flow rather than to underlying T_p. As Davies (1999) pointed out: 'Where the spreading centre is terminated by the transform fault, the sea floor on the other side is at a depth normal for its age. There is no hint of a bulge, due to putative buoyant upwelling under the spreading centre, persisting across the transform fault. This topography is difficult to reconcile with a buoyant upwelling from depth, but is readily explicable if the mid-ocean ridge topography is due to the near surface and local process of conductive cooling, thickening and thermal contraction of the thermal boundary layer (that is, of the lithosphere)' (Davies, 1999, p. 327). The explanation that ridge topography is associated with $F_{OFB,}$ hence T_p, is also inconsistent with the lack of a correlation of ridge depth with Ti_8 (Fig. 13a), because Ti should be as sensitive to F_{OFB} as Na.

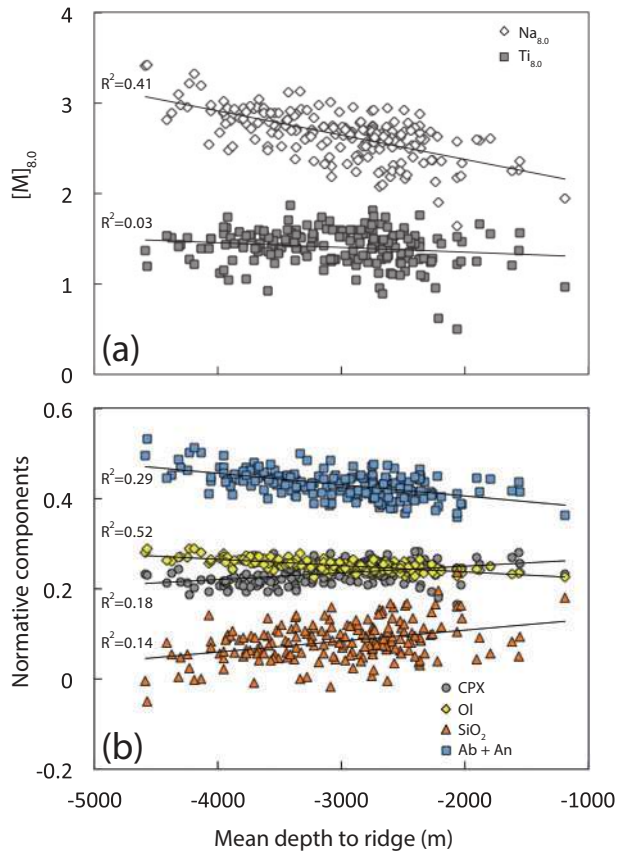

Fig. 13. Variation in (a) Na_8 and Ti_8 versus mean depth to ridge [data presented by Gale *et al.* (2014)] and (b) normative components [see Cox *et al.* (1979) for descriptions of calculations] versus mean depth to ridge (using the filtered 190 ridge sections; see Fig. 10 caption and related text). Normative components are calculated from compositions at 8 wt % MgO from values presented by Gale *et al.* (2014). The comparable decrease in Na_8 and normative Ab + An, yet constant Ti_8 and normative cpx with decreasing mean depth to ridge, indicates that the range in Na_8 of OFB is in part attributable to RMTX magma chambers. (See text for details.)

Possible extenuating circumstances for this were discussed by Langmuir *et al.* (1992). Another suggestion is that topography may reflect large-scale variations in mantle composition (Niu & O'Hara, 2008).

Our finding that variability of Na_8 owing to RMTX processes depends on f_{ol}:f_{cpx}:f_{plag} more sensitively than previously allowed for suggests an alternative hypothesis. The main method used by O'Hara (1965, 1968) to demonstrate that tholeiites (i.e. in this context, OFB) were not primary magmas was their clustering around the low-pressure cotectic. Here we have reduced the projected compositions of ridge segments at MgO = 8 wt % of Gale *et al.* (2014) for 'normal' ridge segments ($n = 190$) to their normative components in the relevant part of the basalt tetrahedron, Ol (M_2SiO_4), Cpx ($CaMSi_2O_6$), Plag ($CaAl_2Si_2O_8 + NaAlSi_3O_8$) and SiO_2, where M = Mg + Fe; these are plotted against ridge depth in Fig. 13b. There is a systematic decrease of normative Plag and especially Ol with decreasing mean depth to the ridge (Fig. 13b), with $R^2 = 0{\cdot}52$ for Ol versus decreasing mean depth to ridge, exceeding that for the correlation of Na_8 versus ridge depth, $R^2 = 0{\cdot}41$ (Fig. 13a). This observation provides another item of evidence that the correlation between basalt chemistry projected onto 8 wt % MgO and ridge depth is due at least in part to the effects of crystallization in RMTX magma chambers. The correlation of normative Cpx with ridge depth is poor ($R^2 = 0{\cdot}18$; Fig. 13b), consistent with the lack of correlation between Ti_8 and ridge depth (Fig. 13a).

In the context of the RMTX model, OFB are not expected to be cotectic compositions but mixtures between the cotectic compositions and the parental liquids. At the average erupted OFB composition of 7·6 wt % MgO, the model of O'Neill & Jenner (2012) for the global average evolution by RMTX of OFB predicts that 56% of the erupted basalt is replenishing parental melt, with only 44% cotectic melt from previous cycles (Fig. 1). However, if we make the limiting assumption that the parental OFB melt has a constant major element composition, such that the trends seen in Fig. 13b are solely due to the changing locus of the cotectic, the trends correlating higher normative Plag and Ol with deeper ridges may correspond to the deeper ridges having higher pressures of cotectic crystallization. This relationship is blurred by the confounding variables discussed previously, namely Na/(Na + Ca) as described by Biggar & Humphries (1981), and normative SiO_2. The latter is much more strongly anticorrelated with normative Plag in these data than expected from the closure effect, indicating a significant dependence of major element cotectic compositions on the magma chamber characteristics of ϕ_X and ϕ_T.

CONCLUSIONS

The recognition by Mike O'Hara that magma chemistry evolves in volcanic systems by processes other than simple fractional crystallization (SFX) has a profound effect on how these chemistries are interpreted. Effects ascribed to mantle processes in the SFX-only paradigm, such as incompatible trace element fractionation by very low degrees of partial melting, find an alternative explanation in RMTX processes, which leads to a different perspective of the causes of trace element variability in the OFB-source mantle. The variability points to an OFB-source mantle that is by no means 'primitive', meaning that it does not have the solar-system relative abundances of refractory lithophile elements expected of Bulk Silicate Earth 'chondritic' models. This is seen both in subtle differences in very incompatible element (VICE) ratios, and in the huge range of VICE to LICE, covering two orders of magnitude. Nevertheless, this chemical differentiation seems to be due to only a few processes. The evidence for this is that ~90% of the normalized variability of 45 incompatible trace elements can be accounted for by only three 'associations of variability' (Fig. 10; Supplementary Data Table 2). Partial melting of this mantle to form the oceanic crust also

appears to be a remarkably uniform process, resulting in little variability in the major element and LICE chemistry of parental basalts (Fig. 3).

Another key observation is the constancy of ratios of certain HICE elements in OFB, particularly (Sm + Gd)/Ti, which are expected to be fractionated by variable degrees of partial melting (Fig. 2c). The constancy of another ratio, P/Pr, which is noteworthy because of the unique property of P among HICE of favouring olivine over pyroxenes, provides additional evidence along similar lines. These constant HICE ratios have further significance. First, whatever processes were responsible for the compositional characteristics of the OFB-source mantle, including the huge range in concentrations of the VICE (Fig. 4) and the non-chondritic ratios among the VICE (Fig. 5), they did not fractionate Ti from (Sm + Gd), nor P from Pr. This is worth remembering whenever a 'low-degree melt' is invoked as a *deus ex machina.* Second, these constant ratios are not consistent with significant heterogeneity in source lithology.

By contrast to its homogeneous lithology, the source composition of OFB, often called the 'Depleted Mantle' or 'Depleted MORB Mantle' (DM or DMM) is very heterogeneous in the most incompatible of the incompatible trace elements, with the variabilities of the VICE in global OFB mostly inherited from this source composition heterogeneity (Fig. 10; i.e. the fraction of variability recovered for the VICE is $>0{\cdot}7$ in $\mathbf{V_1}$, ~ 0 in $\mathbf{V_2}$ and $\leq 0{\cdot}2$ in $\mathbf{V_3}$). For the VICE, the OFB source cannot be regarded other than as a distribution of compositions, with the distribution well described by the log-normal ideal. The average VICE and HICE abundances in the OFB distribution of compositions are depleted relative to chondritic abundances, and are approximately complementary to the continental crust (e.g. Hofmann, 1988). Beyond this broad picture, however, understanding how the distribution of the VICE has come about remains a challenge (Fig. 4). A significant finding of this study is that elements only a little less incompatible than the VICE, namely the HICE and MICE, have variabilities showing entirely different characteristics (Fig. 10). In particular, four elements featuring in radiogenic isotope geochemistry much applied to basalt petrogenetic studies, Nd, Sm, Hf and Lu, have variabilities almost decoupled from those of the VICE, attesting to control by different processes. We suggest, following O'Hara (1977), that these processes include crustal evolution by RMTX. Also conspicuous is the difference in behaviour of the plagioclase-compatible elements Na and Sr (Figs 8–10), which correlate with the magnitude of the Eu anomaly (Fig. 9). As plagioclase is probably not stable in the partial melting regime, this behaviour must point also to crustal processes. In this study we have endeavoured to answer the call made by Mike O'Hara that: 'These effects must be quantified before chemical features of lavas are ascribed to the nature of the underlying upper mantle' (O'Hara, 1977).

SUPPLEMENTARY DATA

Supplementary data for this paper are available at *Journal of Petrology* online.

ACKNOWLEDGEMENTS

We would like to thank Yaoling Niu for inviting us to contribute to the O'Hara (our geochemical hero) thematic issue, and Marjorie Wilson for editorial handling. Mike O'Hara wrote some of our favourite papers and it is an honour to dedicate this paper to him and his family. Yaoling Niu and Laurence Coogan are thanked for their insightful reviews.

REFERENCES

Albarède, F. (1985). Regime and trace-element evolution of open magma chambers. *Nature* **318**, 356–358.

Albarède, F. (1992). How deep do common basaltic magmas form and differentiate?. *Journal of Geophysical Research, B: Solid Earth* **97**, 10997–11009.

Allen, R. M., Nolet, G., Morgan, W. J., Vogfjörd, K., Bergsson, B. H., Erlendsson, P., Foulger, G. R., Jakobsdóttir, S., Julian, B. R., Pritchard, M., Ragnarsson, S. & Stefánsson, R. (2002). Imaging the mantle beneath Iceland using integrated seismological techniques. *Journal of Geophysical Research: Solid Earth* **107**, ESE 3-1–ESE 3-16.

Andersen, M. B., Elliott, T., Freymuth, H., Sims, K. W. W., Niu, Y. & Kelley, K. A. (2015). The terrestrial uranium isotope cycle. *Nature* **517**, 356–359.

Anderson, D. L. (2000). The thermal state of the upper mantle; No role for mantle plumes. *Geophysical Research Letters* **27**, 3623–3626.

Arculus, R. J. (2004). Evolution of arc magmas and their volatiles. In: Sparks, R. S. J. & Hawkesworth, C. J. (eds) *The State of the Planet: Frontiers and Challenges in Geophysics*. International Union of Geodesy and Geophysics; Washington, DC: American Geophysical Union, pp. 95–108.

Arevalo, R. & McDonough, W. F. (2010). Chemical variations and regional diversity observed in MORB. *Chemical Geology* **271**, 70–85.

Asimow, P. D., Dixon, J. E. & Langmuir, C. H. (2004). A hydrous melting and fractionation model for mid-ocean ridge basalts: Application to the Mid-Atlantic Ridge near the Azores. *Geochemistry, Geophysics, Geosystems* **5**, Q01E16.

Bebout, G. E. (2014). Chemical and isotopic cycling in subduction zones. In: Turekian, K. K. & Holland, H. D. (eds) *Treatise on Geochemistry, The Crust*, 2nd edn. Elsevier, pp. 703–747.

Biggar, G. M. & Humphries, D. J. (1981). The plagioclase, forsterite, diopside, liquid equilibrium in the system. *Mineralogical Magazine* **44**, 309–314.

Blichert-Toft, J., Zanda, B., Ebel, D. S. & Albarède, F. (2010). The Solar System primordial lead. *Earth and Planetary Science Letters* **300**, 152–163.

Bown, J. W. & White, R. S. (1994). Variation with spreading rate of oceanic crustal thickness and geochemistry. *Earth and Planetary Science Letters* **121**, 435–449.

Brandl, P. A., Regelous, M., Beier, C., O'Neill, H. St C., Nebel, O. & Haase, K. M. (2016). The timescales of magma evolution at mid-ocean ridges. *Lithos* **240–243**, 49–68.

Bryan, W. B., Thompson, G., Frey, F. A. & Dickey, J. S. (1976). Inferred geologic settings and differentiation in basalts from the Deep-Sea Drilling Project. *Journal of Geophysical Research* **81**, 4285–4304.

Campbell, I. H. (2003). Constraints on continental growth models from Nb/U ratios in the 3.5 Ga Barberton and other Archaean basalt–komatiite suites. *American Journal of Science* **303**, 319–351.

Campbell, I. H. (2007). Testing the plume theory. *Chemical Geology* **24**, 153–176.

Canales, J. P., Ito, G., Detrick, R. S. & Sinton, J. (2002). Crustal thickness along the western Galápagos Spreading Center and the compensation of the Galápagos hotspot swell. *Earth and Planetary Science Letters* **203**, 311–327.

Cann, J. R. (1971). Major element variations in ocean-floor basalts. *Philosophical Transactions of the Royal Society of London, Series A* **268**, 495–505.

Cannat, M. (1996). How thick is the magmatic crust at slow spreading oceanic ridges? *Journal of Geophysical Research* **101**, 2847–2857.

Chauvel, C., Goldstein, S. L. & Hofmann, A. W. (1995). Hydration and dehydration of oceanic crust controls Pb evolution in the mantle. *Chemical Geology* **126**, 65–75.

Christie, D. M. & Sinton, J. M. (1981). Evolution of abyssal lavas along propagating segments of the Galapagos spreading center. *Earth and Planetary Science Letters* **56**, 321–335.

Collerson, K. D. & Kamber, B. S. (1999). Evolution of the continents and the atmosphere inferred from Th–U–Nb systematics of the depleted mantle. *Science* **283**, 1519–1522.

Coogan, L. A. (2014). The lower oceanic crust. In: Turekian, K. K. & Holland, H. D. (eds) *Treatise on Geochemistry*, 2nd edn. Elsevier, pp. 497–541.

Coogan, L. A. & O'Hara, M. J. (2015). MORB differentiation: *In situ* crystallization in replenished–tapped magma chambers. *Geochimica et Cosmochimica Acta* **158**, 147–161.

Cordery, M. J., Davies, G. F. & Campbell, I. H. (1997). Genesis of flood basalts from eclogite-bearing mantle plumes. *Journal of Geophysical Research: Solid Earth* **102**, 20179–20197.

Cox, K. G., Bell, J. D. & Pankhurst, R. J. (1979). *The Interpretation of Igneous Rocks*. Springer.

Dalton, C. A., Langmuir, C. H. & Gale, A. (2014). Geophysical and geochemical evidence for deep temperature variations beneath mid-ocean ridges. *Science* **344**, 80–83.

Danyushevsky, L. V. & Plechov, P. (2011). Petrolog3: Integrated software for modeling crystallization processes. *Geochemistry, Geophysics, Geosystems* **12**, Q07021.

Dasgupta, R., Hirschmann, M. M., McDonough, W. F., Spiegelman, M. & Withers, A. C. (2009). Trace element partitioning between garnet lherzolite and carbonatite at 6·6 and 8·6 GPa with applications to the geochemistry of the mantle and of mantle-derived melts. *Chemical Geology* **262**, 57–77.

Davies, G. F. (1999). *Dynamic Earth: Plates, Plumes and Mantle Convection*. Cambridge University Press.

Davies, G. F. (2011). *Mantle Convection for Geologists*. Cambridge University Press.

DeMets, C. & Wiggins-Grandison, M. (2007). Deformation of Jamaica and motion of the Gonâve microplate from GPS and seismic data. *Geophysical Journal International* **168**, 362–378.

Dick, H. J. B., Lin, J. & Schouten, H. (2003). An ultraslow-spreading class of ocean ridge. *Nature* **426**, 405–412.

Donnelly, K. E., Goldstein, S. L., Langmuir, C. H. & Spiegelman, M. (2004). Origin of enriched ocean ridge basalts and implications for mantle dynamics. *Earth and Planetary Science Letters* **226**, 347–366.

Dungan, M. A. & Rhodes, J. M. (1978). Residual glasses and melt inclusions in basalts from DSDP Legs 45 and 46: Evidence for magma mixing. *Contributions to Mineralogy and Petrology* **67**, 417–431.

Elliott, T., Plank, T., Zindler, A., White, W. & Bourdon, B. (1997). Element transport from slab to volcanic front at the Mariana arc. *Journal of Geophysical Research: Solid Earth* **102**, 14991–15019.

Engel, A. E. J., Engel, C. G. & Havens, R. G. (1965). Chemical characteristics of oceanic basalts and the upper mantle. *Geological Society of America Bulletin* **76**, 719–734.

Falloon, T. J., Danyushevsky, L. V., Ariskin, A., Green, D. H. & Ford, C. E. (2007). The application of olivine geothermometry to infer crystallisation temperatures of parental liquids: implications for the temperatures of MORB magmas. *Chemical Geology* **241**, 207–233.

Francis, D. (1986). The pyroxene paradox in MORB glasses—a signature of picritic parental magmas?. *Nature* **319**, 586–589.

Gale, A., Dalton, C. A., Langmuir, C. H., Su, Y. & Schilling, J.-G. (2013). The mean composition of ocean ridge basalts. *Geochemistry, Geophysics, Geosystems* doi:10.1029/2012gc004334.

Gale, A., Langmuir, C. H. & Dalton, C. A. (2014). The global systematics of ocean ridge basalts and their origin. *Journal of Petrology* **55**, 1051–1082.

Gillis, K. M., Snow, J. E., Klaus, A., et al. (2014). Primitive layered gabbros from fast-spreading lower oceanic crust. *Nature* **505**, 204–207.

Green, D. H., Falloon, T., Eggins, S. M. & Yaxley, G. M. (2001). Primary magmas and mantle temperatures. *European Journal of Mineralogy* **13**, 437–451.

Gregg, P. M., Hebert, L. B., Montési, L. G. J. & Katz, R. F. (2012). Geodynamic models of melt generation and extraction at mid-ocean ridges. *Oceanography* **25**, 78–88.

Hekinian, R. & Walker, D. (1987). Diversity and spatial zonation of volcanic rocks from the East Pacific Rise near 21°N. *Contributions to Mineralogy and Petrology* **96**, 265–280.

Herzberg, C., Asimow, P. D., Arndt, N., Niu, Y., Lesher, C. M., Fitton, J. G., Cheadle, M. J. & Saunders, A. D. (2007). Temperatures in ambient mantle and plumes: Constraints from basalts, picrites, and komatiites. *Geochemistry, Geophysics, Geosystems* **8**, Q02006.

Hirschmann, M. M. (2000). Mantle solidus: Experimental constraints and the effects of peridotite composition. *Geochemistry, Geophysics, Geosystems* **1**, 2000GC000070.

Hirschmann, M. M. & Stolper, E. M. (1996). A possible role for garnet pyroxenite in the origin of the "garnet signature" in MORB. *Contributions to Mineralogy and Petrology* **124**, 185–208.

Hofmann, A. W. (1988). Chemical differentiation of the Earth: the relationship between mantle, continental crust, and oceanic crust. *Earth and Planetary Science Letters* **90**, 297–314.

Hofmann, A. W. (2003). Sampling mantle heterogeneity through oceanic basalts: isotopes and trace elements. In: Carlson, R. W. (ed.) *Treatise on Geochemistry: The Mantle and Core*. Elsevier, pp. 61–101.

Hofmann, A. W. & Jochum, K. P. (1996). Source characteristics derived from very incompatible trace elements in Mauna Loa and Mauna Kea basalts, Hawaii Scientific Drilling Project. *Journal of Geophysical Research* **101**, 11831–11839.

Hofmann, A. W., Jochum, K. P., Seufert, M. & White, W. M. (1986). Nb and Pb in oceanic basalts: new constraints on mantle evolution. *Earth and Planetary Science Letters* **79**, 33–45.

Hotelling, H. (1933). Analysis of a complex of statistical variables into principal components. *Journal of Educational Psychology* **24**, 498–520.

Jenner, F. E. & Arevalo, R. D. (2016). Major and trace element analysis of natural and experimental igneous systems using LA-ICP-MS. *Elements* **12**, 311–316.

Jenner, F. E. & O'Neill, H. St C. (2012a). Analysis of 60 elements in 616 ocean floor basaltic glasses. *Geochemistry, Geophysics, Geosystems* **13**, doi:10.1029/2011GC004009.

Jenner, F. E. & O'Neill, H. St C. (2012b). Major and trace analysis of basaltic glasses by laser-ablation ICP-MS. *Geochemistry, Geophysics, Geosystems* **13**, doi:10.1029/2011GC003890.

Jenner, F. E., O'Neill, H. St C., Arculus, R. J. & Mavrogenes, J. A. (2010). The magnetite crisis in the evolution of arc-related magmas and the initial concentration of Au, Ag, and Cu. *Journal of Petrology* **51**, 2445–2464.

Jenner, F. E., Hauri, E. H., Bullock, E. S., König, S., Arculus, R. J., Mavrogenes, J. A., Mikkelson, N. & Goddard, C. I. (2015). The competing effects of sulfide saturation versus degassing on the behavior of the chalcophile elements during the differentiation of hydrous melts. *Geochemistry, Geophysics, Geosystems* **16**, doi:10.1002/2014GC005670.

Jones, S. M., Murton, B. J., Fitton, J. G., White, N. J., Maclennan, J. & Walters, R. L. (2014). A joint geochemical–geophysical record of time-dependent mantle convection south of Iceland. *Earth and Planetary Science Letters* **386**, 86–97.

Kamenetsky, V. S. & Eggins, S. M. (2012). Systematics of metals, metalloids, and volatiles in MORB melts: Effects of partial melting, crystal fractionation and degassing (a case study of Macquarie Island glasses). *Chemical Geology* **302–303**, 76–86.

Katz, R. F. (2010). Porosity-driven convection and asymmetry beneath mid-ocean ridges. *Geochemistry, Geophysics, Geosystems* **11**, Q0AC07.

Kent, A. J. R. (2008). Melt inclusions in basaltic and related volcanic rocks. In: Putirka, K. D. & Tepley, F. J., III (eds) *Minerals, Inclusions and Volcanic Processes. Mineralogical Society of America and Geochemical Society, Reviews in Mineralogy and Geochemistry* **69**, 273–331.

King, S. D. & Adam, C. (2014). Hotspot swells revisited. *Physics of the Earth and Planetary Interiors* **235**, 66–83.

Klein, E. M. & Langmuir, C. H. (1987). Global correlations of ocean ridge basalt chemistry with axial depth and crustal thickness. *Journal of Geophysical Research* **92**, 8089–8115.

Klein, E. M. & Langmuir, C. H. (1989). Local versus global variations in ocean ridge basalt composition: A reply. *Journal of Geophysical Research: Solid Earth* **94**, 4241–4252.

König, S., Münker, C., Schuth, S. & Garbe-Schönberg, D. (2008). Mobility of tungsten in subduction zones. *Earth and Planetary Science Letters* **274**, 82–92.

Lambart, S., Laporte, D. & Schiano, P. (2013). Markers of the pyroxenite contribution in the major-element compositions of oceanic basalts: Review of the experimental constraints. *Lithos* **160–161**, 14–36.

Lange, R. A. & Carmichael, I. S. E. (1987). Densities of Na_2O–K_2O–MgO–MgO–FeO–Fe_2O_3–Al_2O_3–TiO_2–SiO_2 liquids: New measurements and derived partial molar properties. *Geochimica et Cosmochimica Acta* **51**, 2931–2946.

Langmuir, C. H. (1989). Geochemical consequences of *in situ* crystallization. *Nature* **340**, 199–205.

Langmuir, C. H., Klein, E. M. & Plank, T. (1992). Petrological systematics of mid-ocean ridge basalts: constraints of melt generation beneath ocean ridges. In: Morgan, J. P., Blackman, D. K. & Sinton, J. M. (eds) *Mantle Flow and Melt Generation at Mid-ocean Ridges. American Geophysical Union, Geophysical Monograph* **71**, 183–280.

Le Voyer, M., Cottrell, E., Kelley, K. A., Brounce, M. & Hauri, E. H. (2015). The effect of primary versus secondary processes on the volatile content of MORB glasses: An example from the equatorial Mid-Atlantic Ridge (5°N–3°S). *Journal of Geophysical Research: Solid Earth* **120**, 125–144.

Libourel, G., Boivin, P. & Biggar, G. M. (1989). The univariant curve liquid = forsterite + anorthite + diopside in the system CMAS at 1 bar: solid solutions and melt structure. *Contributions to Mineralogy and Petrology* **102**, 406–421.

Lissenberg, C. J., MacLeod, C. J., Howard, K. A. & Godard, M. (2013). Pervasive reactive melt migration through fast-spreading lower oceanic crust (Hess Deep, equatorial Pacific Ocean). *Earth and Planetary Science Letters* **361**, 436–447.

Louden, K. E., Tucholke, B. E. & Oakey, G. N. (2004). Regional anomalies of sediment thickness, basement depth and isostatic crustal thickness in the North Atlantic Ocean. *Earth and Planetary Science Letters* **224**, 193–211.

Mallmann, G. & O'Neill, H. St C. (2009). The crystal/melt partitioning of V during mantle melting as a function of oxygen fugacity compared with some other elements (Al, P, Ca, Sc, Ti, Cr, Fe, Ga, Y, Zr and Nb). *Journal of Petrology* **50**, 1765–1794.

Mallmann, G., O'Neill, H. St C. & Klemme, S. (2009). Heterogeneous distribution of phosphorus in olivine from otherwise well-equilibrated spinel peridotite xenoliths and its implications for the mantle geochemistry of lithium. *Contributions to Mineralogy and Petrology* **158**, 485–504.

Marsh, B. D. (2007). Magmatism, magma, and magma chambers. In: Schubert, G. (ed.) *Treatise on Geophysics*. Elsevier, pp. 275–333.

McKenzie, D. (1984). The generation and compaction of partially molten rock. *Journal of Petrology* **25**, 713–765.

McKenzie, D. & Bickle, M. J. (1988). The volume and composition of melt generated by extension of the lithosphere. *Journal of Petrology* **29**, 625–679.

Melson, W. G., O'Hearn, T. & Jarosewich, E. (2002). A data brief on the Smithsonian Abyssal Volcanic Glass Data File. *Geochemistry, Geophysics, Geosystems* **3**, 1023, doi:10.1029/2001GC000249.

Niu, Y. (1997). Mantle melting and melt extraction processes beneath ocean ridges; evidence from abyssal peridotites. *Journal of Petrology* **38**, 1047–1074.

Niu, Y. & Batiza, R. (1991). An empirical method for calculating melt compositions produced beneath mid-ocean ridges; for axis and off-axis (seamounts) melting application. *Journal of Geophysical Research, B: Solid Earth* **96**, 21753–21777.

Niu, Y. & O'Hara, M. J. (2008). Global correlations of ocean ridge basalt chemistry with axial depth: a new perspective. *Journal of Petrology* **49**, 633–664.

O'Hara, M. J. (1965). Primary magmas and the origin of basalts. *Scottish Journal of Geology* **1**, 19–40.

O'Hara, M. J. (1968). Are ocean floor basalts primary magmas?. *Nature* **220**, 683–686.

O'Hara, M. J. (1977). Geochemical evolution during fractional crystallisation of a periodically refilled magma chamber. *Nature* **266**, 503–507.

O'Hara, M. J. & Herzberg, C. (2002). Interpretation of trace element and isotope features of basalts: relevance of field relations, petrology, major element data, phase equilibria, and magma chamber modeling in basalt petrogenesis. *Geochimica et Cosmochimica Acta* **66**, 2167–2191.

O'Hara, M. J. & Mathews, R. E. (1981). Geochemical evolution in an advancing, periodically replenished, periodically tapped, continuously fractionated magma chamber. *Journal of the Geological Society, London* **138**, 237–277.

O'Neill, H. St C. (2016). The smoothness and shapes of chondrite-normalized rare earth element patterns in basalts. *Journal of Petrology* **57**, 1463–1508.

O'Neill, H. St C. & Jenner, F. E. (2012). The global pattern of trace-element distributions in ocean floor basalts. *Nature* **491**, 698–704.

O'Neill, H. St C. & Mallmann, G. (2007). The P/Nd ratio of basalt as an indicator of pyroxenite in its source. *Geochimica et Cosmochimica Acta* **71**, Supplement 1:A741.

O'Neill, H. St C. & Palme, H. (1998). Composition of the Silicate Earth: implications for accretion and core formation. In:

Jackson, I. (ed.) *The Earth's Mantle; Composition, Structure, and Evolution*. Cambridge University Press, pp. 3–126.

O'Neill, H. St C. & Palme, H. (2008). Collisional erosion and the non-chondritic composition of the terrestrial planets. *Philosophical Transactions of the Royal Society of London, Series A* **366**, 4205–4238.

Pallister, J. S. (1984). Parent magmas of the Semail ophiolite, Oman. In: Gass, I. G., Lippard, S. J. & Shelton, A. W. (eds) *Ophiolites and Oceanic Lithosphere. Geological Society, London, Special Publications* **13**, 63–70.

Palme, H., Lodders, K. & Jones, A. (2014). Solar System abundances of the elements. In: Turekian, K. K. & Holland, H. D. (eds) *Treatise on Geochemistry*, 2nd edn. Elsevier, pp. 15–36.

Parnell-Turner, R., White, N., Henstock, T., Murton, B., Maclennan, J. & Jones, S. M. (2014). A continuous 55-million-year record of transient mantle plume activity beneath Iceland. *Nature Geoscience* **7**, 914–919.

Patten, C., Barnes, S.-J., Mathez, E. A. & Jenner, F. E. (2013). Partition coefficients of chalcophile elements between sulfide and silicate melts and the early crystallization history of sulfide liquid: LA-ICP-MS analysis of MORB sulfide droplets. *Chemical Geology* **358**, 170–188.

Pearce, J. A., Stern, R. C., Bloomer, S. H. & Fryer, P. (2005). Geochemical mapping of the Mariana arc–basin system: Implications for the nature and distribution of subduction components. *Geochemistry, Geophysics, Geosystems* **6**, Q07006, doi:10.1029/2004GC000895.

Perfit, M. R., Gust, D. A., Bence, A. E., Arculus, R. J. & Taylor, S. R. (1980). Chemical characteristics of island-arc basalts; implications for mantle sources. *Chemical Geology* **30**, 227–256.

Perfit, M. R., Fornari, D. J., Malahoff, A. & Embley, R. W. (1983). Geochemical studies of abyssal lavas recovered by DSRV *Alvin* from Eastern Galapagos Rift, Inca Transform, and Ecuador Rift: 3. Trace element abundances and petrogenesis. *Journal of Geophysical Research* **88**, 10551–10572.

Pirard, C., Hermann, J. & O'Neill, H. St C. (2013). Petrology and geochemistry of the crust–mantle boundary in a nascent arc, Massif du Sud Ophiolite, New Caledonia, SW Pacific. *Journal of Petrology* **54**, 1759–1792.

Plank, T. (2014). The chemical composition of subducting sediments. In: Turekian, K. K. & Holland, H. D. (eds) *Treatise on Geochemistry, The Crust*, 2nd edn. Elsevier, pp. 607–629.

Poore, H. R., White, N. & Jones, S. (2009). A Neogene chronology of Iceland plume activity from V-shaped ridges. *Earth and Planetary Science Letters* **283**, 1–13.

Presnall, D. C., Dixon, S. A., Dixon, J. R., O'Donnell, T. H., Brenner, N. L., Schrock, R. L. & Dycus, D. W. (1978). Liquidus phase relations on the join diopside–forsterite–anorthite from 1 atm to 20 kbar: Their bearing on the generation and crystallization of basaltic magma. *Contributions to Mineralogy and Petrology* **66**, 203–220.

Putirka, K. D. (2008). Thermometers and barometers for volcanic systems. In: Putirka, K. D. & Tepley, F. J., III (eds) *Minerals, Inclusions and Volcanic Processes. Mineralogical Society of America and Geochemical Society, Reviews in Mineralogy and Geochemistry* **69**, 61–120.

Putirka, K. D., Perfit, M., Ryerson, F. J. & Jackson, M. G. (2007). Ambient and excess mantle temperatures, olivine thermometry, and active vs. *passive upwelling.* Chemical Geology **241**, 177–206.

Rhodes, J. M., Dungan, M. A., Blanchard, D. P. & Long, P. E. (1979). Magma mixing at mid-ocean ridges: Evidence from basalts drilled near 22°N on the Mid-Atlantic Ridge. *Tectonophysics* **55**, 35–61.

Roeder, P., Gofton, E. & Thornber, C. (2006). Cotectic proportions of olivine and spinel in olivine-tholeiitic basalt and evaluation of pre-eruptive processes. *Journal of Petrology* **47**, 883–900.

Rubin, K. H. & Sinton, J. M. (2007). Inferences on mid-ocean ridge thermal and magmatic structure from MORB compositions. *Earth and Planetary Science Letters* **260**, 257–276.

Rubin, K. H., Smith, M. C., Bergmanis, E. C., Perfit, M. R., Sinton, J. M. & Batiza, R. (2001). Geochemical heterogeneity within mid-ocean ridge lava flows: insights into eruption, emplacement and global variations in magma generation. *Earth and Planetary Science Letters* **188**, 349–367.

Rudnick, R. L. & Gao, S. (2003). Composition of the continental crust. In: Rudnick, R. L. (ed.) *Treatise on Geochemistry: The Crust*. Elsevier, pp. 1–64.

Salters, V. J. M. & Hart, S. R. (1989). The hafnium paradox and the role of garnet in the source of mid-ocean-ridge basalts. *Nature* **342**, 420–422.

Salters, V. J. M. & Stracke, A. (2004). Composition of the depleted mantle. *Geochemistry, Geophysics, Geosystems* **5**, doi:10.1029/2003GC000597.

Schilling, J. G. (1973). Iceland mantle plume: geochemical study of Reykjanes Ridge. *Nature* **242**, 565–571.

Schilling, J. G. (1975). Azores mantle blob: Rare-earth evidence. *Earth and Planetary Science Letters* **25**, 103–115.

Scott, D. R. & Stevenson, D. J. (1986). Magma ascent by porous flow. *Journal of Geophysical Research* **91**, 9283–9296.

Searle, M. & Cox, J. (1999). Tectonic setting, origin, and obduction of the Oman ophiolite. *Geological Society of America Bulletin* **111**, 104–122.

Shorttle, O. (2015). Geochemical variability in MORB controlled by concurrent mixing and crystallisation. *Earth and Planetary Science Letters* **424**, 1–14.

Sinton, J. M. & Detrick, R. S. (1992). Mid-ocean ridge magma chambers. *Journal of Geophysical Research: Solid Earth* **97**, 197–216.

Sinton, J. M., Wilson, D. S., Christie, D. M., Hey, R. N. & Delaney, J. R. (1983). Petrologic consequences of rift propagation on oceanic spreading ridges. *Earth and Planetary Science Letters* **62**, 193–207.

Sobolev, A. V., Hofmann, A. W., Kuzmin, D. V., et al. (2007). The amount of recycled crust in sources of mantle-derived melts. *Science* **316**, 412–417.

Spandler, C., Mavrogenes, J. & Hermann, J. (2007). Experimental constraints on element mobility from subducted sediments using high-*P* synthetic fluid/melt inclusions. *Chemical Geology* **239**, 228–249.

Sparks, R. S. J., Meyer, P. & Sigurdsson, H. (1980). Density variation amongst mid-ocean ridge basalts: Implications for magma mixing and the scarcity of primitive lavas. *Earth and Planetary Science Letters* **46**, 419–430.

Staudigel, H. (2014). Chemical fluxes from hydrothermal alteration of the oceanic crust. In: Holland, H. D. & Turekian, K. K. (eds) *Treatise on Geochemistry, The Crust*, 2nd edn. Elsevier, pp. 583–606.

Stolper, E. (1980). A phase diagram for mid-ocean ridge basalts: Preliminary results and implications for petrogenesis. *Contributions to Mineralogy and Petrology* **74**, 13–27.

Stracke, A. (2012). Earth's heterogeneous mantle: A product of convection-driven interaction between crust and mantle. *Chemical Geology* **330–331**, 274–299.

Stroup, J. B. & Fox, P. J. (1981). Geologic investigations in the Cayman Trough: evidence for thin oceanic crust along the Mid-Cayman Rise. *Journal of Geology* **89**, 395–420.

Su, W. & Buck, W. R. (1993). Buoyancy effects on mantle flow under mid-ocean ridges. *Journal of Geophysical Research: Solid Earth* **98**, 12191–12205.

Sun, W., Hu, Y., Kamenetsky, V. S., Eggins, S. M., Chen, M. & Arculus, R. J. (2008). Constancy of Nb/U in the mantle revisited. *Geochimica et Cosmochimica Acta* **72**, 3542–3549.

Tippett, L. H. C. (1925). On the extreme individuals and the range of samples taken from a normal population. *Biometrika* **17**, 364–387.

Turner, J. S. & Campbell, I. H. (1986). Convection and mixing in magma chambers. *Earth-Science Reviews* **23**, 255–352.

Turner, S., Hawkesworth, C., Rogers, N. & King, P. (1997). U–Th isotope disequilibria and ocean island basalt generation in the Azores. *Chemical Geology* **139**, 145–164.

Vogt, P. R. (1971). Asthenosphere motion recorded by the ocean floor south of Iceland. *Earth and Planetary Science Letters* **13**, 153–160.

Wade, J. & Wood, B. J. (2001). The Earth's 'missing' niobium may be in the core. *Nature* **409**, 75–78.

Wanless, V. D., Shaw, A. M., Behn, M. D., Soule, S. A., Escartín, J. & Hamelin, C. (2015). Magmatic plumbing at Lucky Strike volcano based on olivine-hosted melt inclusion compositions. *Geochemistry, Geophysics, Geosystems* **16**, 126–147.

Whitaker, M. L., Nekvasil, H., Lindsley, D. H. & Difrancesco, N. J. (2007). The role of pressure in producing compositional diversity in intraplate basaltic magmas. *Journal of Petrology* **48**, 365–393.

White, R. S., McKenzie, D. & O'Nions, R. K. (1992). Oceanic crustal thickness from seismic measurements and rare earth element inversions. *Journal of Geophysical Research* **97**, 19683–19715.

White, R. S., Minshull, T. A., Bickle, M. J. & Robinson, C. J. (2001). Melt generation at very slow-spreading oceanic ridges: constraints from geochemical and geophysical data. *Journal of Petrology* **42**, 1171–1196.

White, W. M. & Bryan, W. B. (1977). Sr-isotope, K, Rb, Cs, Sr, Ba, and rare-earth geochemistry of basalts from the FAMOUS area. *Geological Society of America Bulletin* **88**, 571–576.

White, W. M. & Klein, E. M. (2014). Composition of the oceanic crust. In: Turekian, K. K. & Holland, H. D. (eds) *Treatise on Geochemistry*, 2nd edn. The Crust. Elsevier, pp. 457–496.

White, W. M. & Schilling, J.-G. (1978). The nature and origin of geochemical variation in Mid-Atlantic Ridge basalts from the Central North Atlantic. *Geochimica et Cosmochimica Acta* **42**, 1501–1516.

Witt-Eickshen, G. & O'Neill, H. St C. (2005). The effect of temperature on the equilibrium distribution of trace elements between clinopyroxene, orthopyroxene, olivine and spinel in upper mantle. *Chemical Geology* **221**, 65–101.

Yao, L., Sun, C. & Liang, Y. (2012). A parameterized model for REE distribution between low-Ca pyroxene and basaltic melts with applications to REE partitioning in low-Ca pyroxene along a mantle adiabat and during pyroxenite-derived melt and peridotite interaction. *Contributions to Mineralogy and Petrology* **164**, 261–280.

Yoder, H. S. & Tilley, C. E. (1962). Origin of basalt magmas: an experimental study of natural and synthetic rock systems. *Journal of Petrology* **3**, 342–532.